**AD-A259 221**

OPTICAL MEASUREMENTS IN ELECTRIC FIELDS

Larry P. Goss, Ph.D.

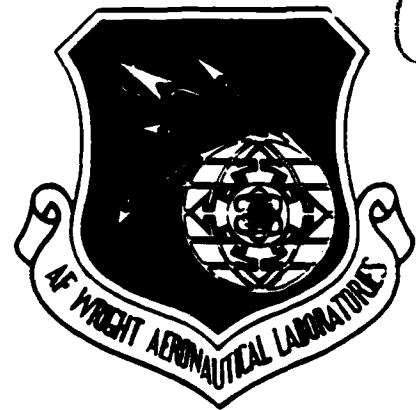Research Applications Division
Systems Research Laboratories, Inc.
2800 Indian Ripple Road
Dayton, OH 45440-3696

DTIC
S ELECTE
JAN 12 1993
B D

May 1987

Final Report for Period 20 September 1982 - 1 September 1986

93-00056

93 1 04 222

# NOTICE

WHEN GOVERNMENT DRAWINGS, SPECIFICATIONS, OR OTHER DATA ARE USED FOR ANY PURPOSE OTHER THAN IN CONNECTION WITH A DEFINITELY GOVERNMENT-RELATED PROCUREMENT, THE UNITED STATES GOVERNMENT INCURS NO RESPONSIBILITY OR ANY OBLIGATION WHATSOEVER. THE FACT THAT THE GOVERNMENT MAY HAVE FORMULATED OR IN ANY WAY SUPPLIED THE SAID DRAWINGS, SPECIFICATIONS, OR OTHER DATA, IS NOT TO BE REGARDED BY IMPLICATION, OR OTHERWISE IN ANY MANNER CONSTRUED, AS LICENSING THE HOLDER, OR ANY OTHER PERSON OR CORPORATION; OR AS CONVEYING ANY RIGHTS OR PERMISSION TO MANUFACTURE, USE, OR SELL ANY PATENTED INVENTION THAT MAY IN ANY WAY BE RELATED THERETO.

This report is releasable to the National Technical Information Service (NTIS). At NTIS, it will be available to the general public, including foreign nations.

THIS TECHNICAL REPORT HAS BEEN REVIEWED AND IS APPROVED FOR PUBLICATION.


SIGMUND W. KIZIRNIS
Power Components Branch
Aerospace Power Division
Aero Propulsion Directorate

LOWELL D. MASSIE
Chief, Power Component Branch
Aerospace Power Division
Aero Propulsion and Power Directorate

FOR THE COMMANDER


MICHAEL D. BRAYDICH, Lt/Col, USAF
Deputy Director
Aerospace Power Division
Aero Propulsion & Power Directorate

IF YOUR ADDRESS HAS CHANGED, IF YOU WISH TO BE REMOVED FROM OUR MAILING LIST, OR IF THE ADDRESSEE IS NO LONGER EMPLOYED BY YOUR ORGANIZATION PLEASE NOTIFY WL/POOC-3____, WRIGHT-PATTERSON AFB, OH 45433-_6563_ TO HELP MAINTAIN A CURRENT MAILING LIST.

COPIES OF THIS REPORT SHOULD NOT BE RETURNED UNLESS RETURN IS REQUIRED BY SECURITY CONSIDERATIONS, CONTRACTUAL OBLIGATIONS, OR NOTICE ON A SPECIFIC DOCUMENT.

# REPORT DOCUMENTATION PAGE

| 1a. REPORT SECURITY CLASSIFICATION | | | 1b. RESTRICTIVE MARKINGS | | | |
|---|---|---|---|---|---|---|
| UNCLASSIFIED | | | | | | |

| 2a. SECURITY CLASSIFICATION AUTHORITY | 3. DISTRIBUTION/AVAILABILITY OF REPORT |
|---|---|
| | Approved for public release; distribution unlimited. |
| 2b. DECLASSIFICATION/DOWNGRADING SCHEDULE | |

| 4. PERFORMING ORGANIZATION REPORT NUMBER(S) | 5. MONITORING ORGANIZATION REPORT NUMBER(S) |
|---|---|
| 6775 Final | AFWAL TR-87-2032 |

| 6a. NAME OF PERFORMING ORGANIZATION | 6b. OFFICE SYMBOL (If applicable) | 7a. NAME OF MONITORING ORGANIZATION |
|---|---|---|
| Research Applications Div. Systems Research Labs., Inc. | | Aero Propulsion Laboratory (AFWAL/POOC-3) |

| 6c. ADDRESS (City, State and ZIP Code) | 7b. ADDRESS (City, State and ZIP Code) |
|---|---|
| 2800 Indian Ripple Road Dayton, OH 45440-3696 | Wright-Patterson Air Force Base, OH 45433-6563 |

| 8a. NAME OF FUNDING/SPONSORING ORGANIZATION | 8b. OFFICE SYMBOL (If applicable) | 9. PROCUREMENT INSTRUMENT IDENTIFICATION NUMBER |
|---|---|---|
| | | F33615-82-C-2231 |

| 8c. ADDRESS (City, State and ZIP Code) | 10. SOURCE OF FUNDING NOS. | | | |
|---|---|---|---|---|
| | PROGRAM ELEMENT NO. | PROJECT NO. | TASK NO. | WORK UNIT NO. |
| | 61102F | 2301 | S1 | 21 |

**11. TITLE (Include Security Classification)**
OPTICAL MEASUREMENTS IN ELECTIC FIELDS (UNCL)

**12. PERSONAL AUTHOR(S)**
Larry P. Goss

| 13a. TYPE OF REPORT | 13b. TIME COVERED | 14. DATE OF REPORT (Yr., Mo., Day) | 15. PAGE COUNT |
|---|---|---|---|
| Final | FROM 20 Sept 82 TO 1 Sept 86 | 1987 May | 54 |

**16. SUPPLEMENTARY NOTATION**

| 17. | COSATI CODES | | 18. SUBJECT TERMS (Continue on reverse if necessary and identify by block number) |
|---|---|---|---|
| FIELD | GROUP | SUB. GR. | Stark Effect, Electric Fields, Plasmas, Laser-Induced Fluorescence, Optogalvanic, Optical Diagnostics, Polarization Spectroscopy, Positive-Column Discharge, Hollow-Cathode (cont) |
| 20 | 06 | | |
| 20 | 09 | | |

**19. ABSTRACT (Continue on reverse if necessary and identify by block number)**

The results of a theoretical and experimental investigation of laser-based diagnostic techniques for the measurement of electric fields in discharges are presented. A theoretical assessment made of those techniques most likely to be successful in electric-field measurements under various plasma conditions is discussed. The three techniques identified and subsequently tested experimentally were polarization spectroscopy of H-atoms, optogalvanic spectroscopy of Rydberg states, and laser-induced fluorescence of the BCl radical. The most successful demonstration of the electric-field measurement involved the optogalvanic technique because of the high sensitivity of the Rydberg states to electric fields. Electric field measurements were made on a hollow cathode in the range 1800 to 200 V/cm.

| 20. DISTRIBUTION/AVAILABILITY OF ABSTRACT | 21. ABSTRACT SECURITY CLASSIFICATION |
|---|---|
| UNCLASSIFIED/UNLIMITED ☒ SAME AS RPT. ☐ DTIC USERS ☐ | Unclassified |

| 22a. NAME OF RESPONSIBLE INDIVIDUAL | 22b. TELEPHONE NUMBER (Include Area Code) | 22c. OFFICE SYMBOL |
|---|---|---|
| S. Kizirnis | (513) 255-2923 | AFWAL/POOC-3 |

**DD FORM 1473, 83 APR**     EDITION OF 1 JAN 73 IS OBSOLETE.

18. Subject Terms (Continued)

Discharge, Rydberg States

# Preface

This report was prepared by Dr. L. P. Goss and covers work performed under Air Force Contract F33615-82-C-2231. Others contributing to this effort were Drs. E. G. Jones and B. G. MacDonald and Messrs. B. Sarka and R. A. Olson. The contract was administered under the direction of the Air Force Wright Aeronautical Laboratories, Aero Propulsion Laboratory (AFWAL/POOC-3), Wright-Patterson Air Force Base, OH, with Mr. S. Kizirnis as Government Project Monitor.

| Accession For | | |
|---|---|---|
| NTIS GRA&I | | ☑ |
| DTIC TAB | | ☐ |
| Unannounced | | ☐ |
| Justification | | |
| By | | |
| Distribution/ | | |
| Availability Codes | | |
| Dist | Avail and/or Special | |
| A-1 | | |

TABLE OF CONTENTS

# LIST OF ILLUSTRATIONS

# Section 1

## INTRODUCTION

This report describes the results of experimental and theoretical investigations of laser-based advanced diagnostic techniques for the measurement of electric fields in discharges.

The U. S. Air Force has a continuing interest in understanding the plasmas which serve as the active media in devices such as gas-discharge lasers and high-power switches for high-repetition-rate pulsed power systems. Operation of these devices at higher power and rep rate is generally curtailed by the development of arcs which originate in the electrode sheaths. Arc-free operation at higher-rep-rate levels will require a better understanding of the nature of these sheaths which can be accomplished through study of the electric field in the sheath; the electric field is the only plasma parameter which is related both to the applied voltage and to the charged-particle densities. In the past, the measurement of the electric field in a plasma was accomplished by means of probe devices. Such devices can disturb the plasma and result in biased measurements due to chemical reactions, impurities, and secondary electrons emitted from the probe surface.

Because of the shortcomings of probe devices, this study was initiated to assess the possibility of using nonintrusive laser probes for measurement of the electric field. The objectives of this study were twofold: first, to conduct a theoretical study of at least three promising methods of measuring electric fields within a plasma medium and, second, to assess experimentally the performance of one or more of these techniques in an appropriate discharge.

In Section 2 of this report, the theoretical assessment of the most promising laser diagnostic techniques is described. Section 3 discusses the experimental evaluation of three techniques including polarization spectroscopy, optogalvanic spectroscopy of Rydberg states, and laser-induced fluorescence of BCl.

1

## Section 2

## THEORETICAL ASSESSMENT

A measurement of the electric field by a spectroscopic technique generally implies that the Stark effect is being employed. Consequently, a detailed discussion of the Stark effect is given in Section 2.1. Important limitations on the measurement techniques arise from various line-broadening effects; these are described in Section 2.2. Section 2.3 reviews diagnostic techniques and assesses the "best" techniques. Section 2.4 discusses the technique selection and limitations.

## 2.1 Stark Effect

In an electric field, the normal components of a spectrum are split by the field perturbation. Figure 1 is a vector diagram illustrating the Stark effect. The electric field induces a dipole moment in the atomic or molecular species. The interaction between the dipole and the field causes a precession of J, the angular-momentum vector, about the applied field such that the $m_j$ components of angular momentum are a constant of motion. Changing the direction of rotation of J has no effect upon the magnitude of the dipole; therefore, the energy shift is the same for $+ m_j$ and $- m_j$. The values of the Stark shift can be deduced from quantum-mechanical calculations by constructing the perturbation Hamiltonian, using the perturbation operator eFz, where e is the charge on the electron, F the field strength, and z the coordinate of the atom in the field, or z the direction.

Results of such a calculation show that hydrogen is a special case. Because of the near degeneracy (a small splitting exists from relativistic effects) of different $\ell$ levels having the same n quantum number, the shifts in Stark components are quite large and linear as a function of electric field. It can also be shown that the selection rules for spectroscopic transitions in the presence of an electric field are $\Delta m_j = 0, \neq 1$.

Figure 1.    Space Quantization of Atom in Applied
            $\vec{E}$ Field.  Note that the polarization is
            independent of the direction of rotation;
            therefore, $+ m_J = - m_J$.

For hydrogen, the presence of an electric field also modifies the
potential of the electron:

$$V = -e^2/4\pi\epsilon_o\alpha - eFz \qquad\qquad (1)$$

where $\epsilon$ is the permittivity of free space and $\alpha$ is the Bohr radius.
The additional potential results in a lowering of the ionization
potential to

$$V' = Z_e (eFz)^{1/2} \qquad\qquad (2)$$

As a result of the lowering of the ionization potential, the rate of
autoionization is increased and could, in principle, be observed as
an increase in line broadening in the presence of the field or as an
increase in electron current.[1]

3

In addition to hydrogen, molecular species[2] in some electronic state other than a $\Sigma$ state and possessing a permanent dipole moment also show a linear Stark shift, given by

$$\Delta E = \frac{\mu \, m_J \Lambda F}{J(J + 1)} \tag{3}$$

where $\mu$ is the dipole moment and $\Lambda$ the electronic angular momentum.

All other species (at "low" fields) show a quadratic Stark effect; i.e., the Stark splitting depends on the square of the electric field. Perturbation theory[3] shows that the line displacement decreases with $m^2$; therefore, each level is split into several components. The magnitude of the effects is smaller for heavier atoms because the $\ell$ levels for the same n quantum numbers are more strongly split. Additionally, the electric field mixes levels of opposite parity, resulting in a breakdown of the $\ell$ selection rule. Transitions for $\Delta \ell = 0$, $\pm 2$, $\pm 3$ are observed in the presence of a field.

Figure 2 contains the energy-level diagrams for the n = 2 and n = 3 levels of hydrogen in the presence of an electric field based on techniques due to Lüders.[4] Figure 3 shows similar calculations for He, based on the method of Foster.[5] The magnitude of the line splits in He for higher values of n can be approximated from[3]

$$\Delta E = (F/F_o)^2 \tag{4}$$

where F is the field in question and $F_o$ is the field required to shift the line components by 1 cm$^{-1}$.

Reference 3 provides the constants for calculating $F_o$. The value of $F_o$ is proportional to $n^{3.5}$. Table 1 contains values for a number of triplet transitions in He.
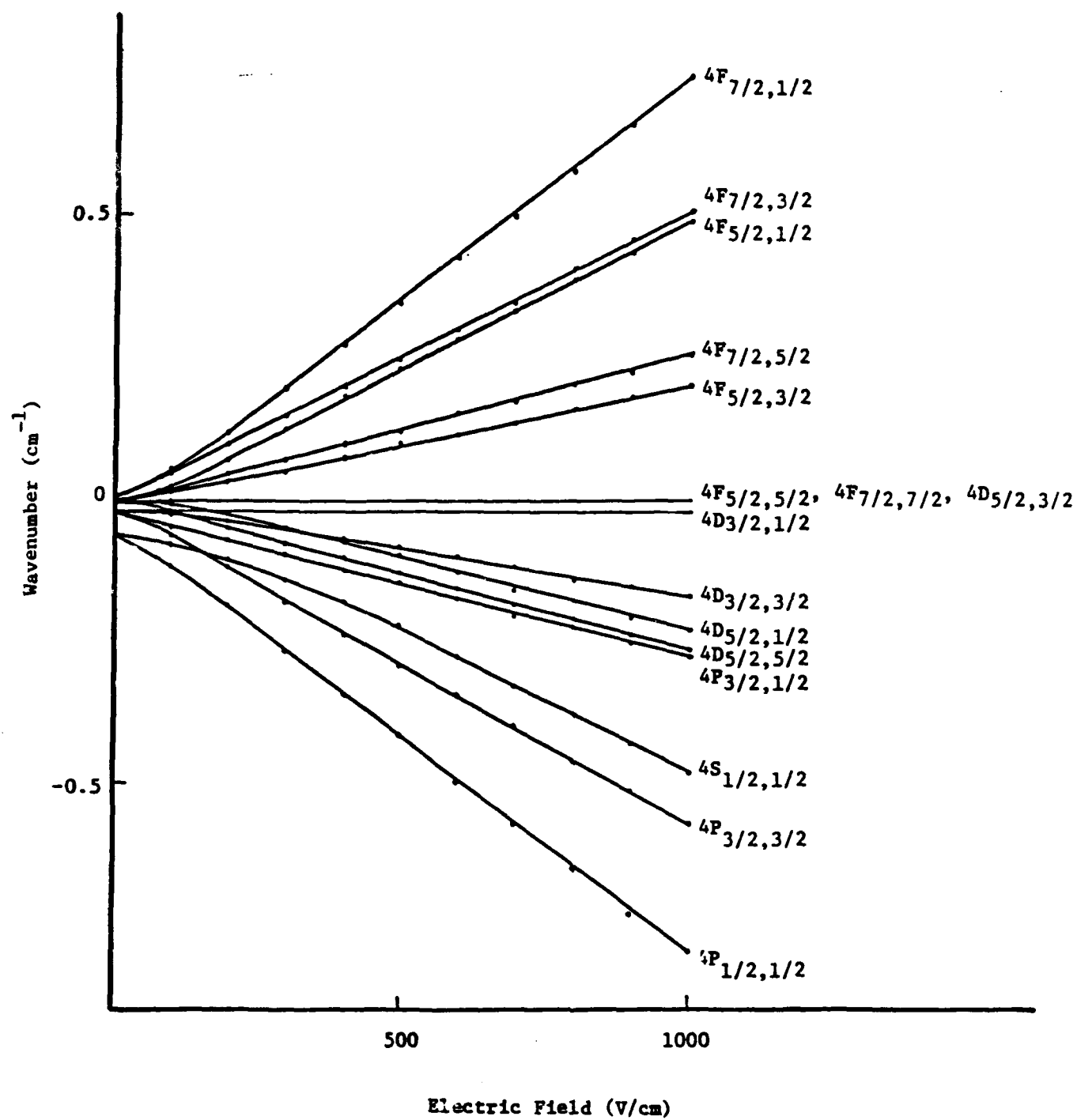
Figure 2. n = 4 Level of Hydrogen, Zero = 102823.910018 cm$^{-1}$.

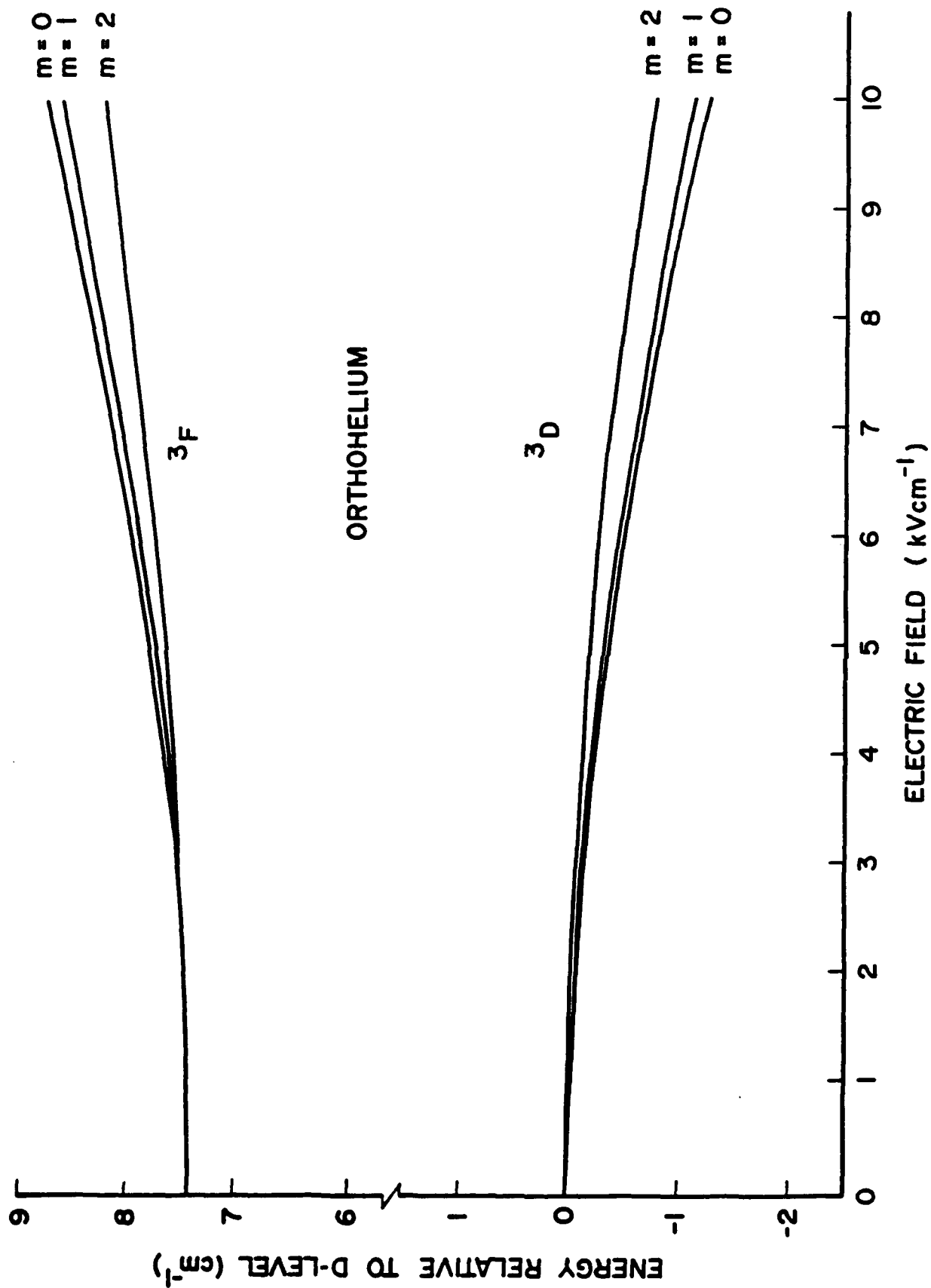Figure 3. $2^3S - 4^3L$ Levels in He.

ORTHOHELIUM

ELECTRIC FIELD ( kVcm$^{-1}$ )

ENERGY RELATIVE TO D-LEVEL (cm$^{-1}$)

$^3F$

$^3D$

m=0
m=1
m=2

m=2
m=1
m=0

6

## TABLE 1

### $F_o$ (in kV/cm) FOR SOME He TRANSITIONS

| n | $^3S$ | $^3P$ | $^3D$ |
|---|-------|-------|-------|
| 4 | 52    | 42    | 8.3   |
| 5 | 23    | 17.5  | 3.3   |
| 6 | 12    | 9     | 1.65  |
| 7 | 6.5   | 4.9   | 0.73  |
| 8 | 4.1   | 3.1   | 0.45  |
| 9 | 2.7   | 2.0   | 0.30  |

## 2.2 Transition Linewidths[6]

The ability to resolve Stark splitting is ultimately determined by
the resolving power of the spectroscopic technique employed and the
linewidths of the spectroscopic transition to be investigated. The
three major components of the spectroscopic linewidths are the natural
linewidth, the Doppler-broadened linewidth, and the collision linewidth.

The natural linewidth arises because species in an excited state decay
with a radiative decay constant $1/A$, where A is the Einstein coefficient.
By performing the Fourier transform of the temporal decay constant to
the frequency domain, it can be shown that the natural linewidth is
a Lorentzian profile given by

$$\delta(\omega) = 1/2\pi \frac{\gamma}{(\omega - \omega_o) + (\gamma/2)^2} \tag{5}$$

where $\omega_o$ is the frequency of the transition and $\alpha$ the damping constant
$(1/A)$. The halfwidth is given by

$$\Delta\nu_N = \gamma/2\pi \tag{6}$$

where $\Delta\nu_N$ is the natural halfwidth in frequency units. For fully allowed visible transitions, lifetimes are on the order of 10 - 100 nsec, which yields natural linewidths on the order of 15 - 1.5 MHz. Natural linewidths become much smaller in the infrared and microwave regions because lifetimes are much longer.

The Doppler width arises from the natural thermal motion of absorbers or emitters. A transition with central frequency $\omega_o$ will absorb light at

$$\omega = \omega_o + \bar{K} \cdot \bar{v} \tag{7}$$

where $\bar{K}$ is the wave vector of the radiation field and $\bar{v}$ the velocity vector of the absorber (or emitter). Since the natural thermal motion of a gaseous medium can be described by a Maxwellian distribution, it can be shown that the Doppler-broadened spectral line is a Gaussian profile given by

$$I(\omega) = I_o \exp\left[-\frac{C(\omega - \omega_o)^2}{\omega_o v_p}\right] \tag{8}$$

where $v_p$ is the gas-kinetic most probable velocity. The halfwidth of a Doppler-broadened profile is given by

$$\nu_D = 7.16 \times 10^{-7} \nu_o \sqrt{T/M} \text{ sec}^{-1} \tag{9}$$

where $\nu_o$ is the central frequency, T the temperature, and M the mole weight. The Doppler width is large for light species such as H. For example, the Doppler halfwidth of $H_\beta$ at room temperature is 7.65 GHz (0.255 cm$^{-1}$). Because it is directly proportional to $\nu_o$, the Doppler width is much smaller for infrared and microwave transitions.

In addition to the Doppler linewidth, another effect which results in line broadening occurs in Doppler-free laser techniques which employ counterpropagating beams. These techniques eliminate the Doppler width by sampling only absorbers with a velocity perpendicular to the wave vector of the radiation field. Since these species are moving

8

across the radiation field, they acquire an additional damping term
as they leave the driving field. Transit time broadening is given by

$$\Delta\nu = 0.37 \ v/W \tag{10}$$

where v is the velocity and W the width of the radiation field (laser
beam). For H at 400 K in a laser focal volume of diameter 0.01 cm, tran-
sit time broadening is $\sim$ 10 MHz.

Collisional line broadening arises from both elastic and inelastic
collisions. In inelastic collisions, internal energy is transferred
during the collision process. These collisions are also called quench-
ing collisions and appear in the line shape as a damping term in
addition to the natural lifetime. This broadening is pressure depend-
ent and may be represented by

$$\Delta\nu = a + bp \tag{11}$$

where a is the natural linewidth, b is the pressure-broadening coeffi-
cient, and p is the pressure.

An additional broadening term arises from elastic collisions. In
these collisions, only translational energy can be exchanged. In this
case, the collision does not act as an additional damping mechanism;
instead, it disturbs the phase of the radiating oscillator. It can
be shown by Fourier analysis that this results in a line halfwidth
given by

$$\Delta\nu = 2N\bar{v}\sigma \tag{12}$$

where N is the number density of the collision partners, $\bar{v}$ the mean
relative velocity, and $\sigma$ the elastic-collision cross section.

9

## 2.3  Review of Optical Diagnostic Techniques

### 2.3.1  Laser-Induced-Fluorescence Spectroscopy

In this very basic technique, a laser pumps some transition and
the resulting fluorescence spectrum is recorded on a monochromator.
This technique can be used to measure electric-field distributions by
observing the relative intensity of field-induced forbidden transitions.[3]
For example, a specific application would be to pump the He $2^1P \rightarrow 4^1S$
transition at 504.7 nm.  One could then monitor the resulting fluores-
cence intensity of the resonance fluorescence at 504.7 and the intensity
of the field-induced forbidden transition from $4^1S \rightarrow 2^1S$.  The major
drawback of this approach is the low sensitivity to electric fields of
the forbidden components accessible by this pumping scheme.  For the
specific transitions just described, a field of 50 kV/cm is required
if the forbidden component is to have 10% of the oscillator strength
of the allowed component.  Consequently, this scheme suffers from low
field sensitivity and is not considered to be a good general approach.

### 2.3.2  Laser-Induced-Fluorescence Excitation Spectroscopy

In this technique, the laser is scanned across absorption features, and
the total fluorescence or a fixed fraction of the total fluorescence
is monitored as a function of excitation wavelength.  This technique is
not limited to fluorescence signals arising from a common upper level
as in the previous method and, consequently, can access more favorable
forbidden transitions.  For example, one could tune the laser to the
$4^1D \rightarrow 2^1P$ transition and monitor the resonance fluorescence intensity
and then tune the laser to the $4^1F \rightarrow 2^1P$ forbidden transition and again
monitor the resonance fluorescence.  The two transitions are separated
only by 0.07 nm; therefore, the fluorescence could be monitored easily
with a single interference filter.

The forbidden component has approximately 10% of the intensity of the
allowed component at about 5 kV/cm and, with care, fields down to
3 kV/cm could be measured. The lower limit could be further enhanced
by going to higher n, since the magnitude is proportional to $n^2$.
Also it should be noted that although only examples of He have been
discussed, similar schemes can be divised for other species.

There are several important drawbacks to the application of this approach,
however. The first is that the overall sensitivity of the experiment
will be determined by the amount of scattered laser light. This limita-
tion is expected to be most severe when the laser is probing near the
electrodes. The second problem is that the quenching rate constants of
the upper levels of allowed and forbidden transitions must be known and
corrected for quenching to determine their relative fluorescence yields.
Assuming, however, that the experimental difficulties can be overcome,
laser-induced-fluorescence excitation spectroscopy is a viable approach
for electric fields above 3 kV/cm and at pressures where quenching is
not important (less than 10 Torr).

An alternative approach employs the BCl radical to indicate the magni-
tude of the electric field.[6] In this method, the electric field induces
mixing between diatomic rotational energy levels of opposite parity.
This mixing manifests itself by the appearance of fluorescent lines
which are forbidden in the absence of an external field. Moore, et
al.,[6] reported making electric-field measurements as small as ∿ 40 V/cm
with high temporal and spatial resolution. The advantage of this tech-
nique is the high sensitivity of the fluorescence signal to the applied
field. The LIF signal in sub-Torr discharges is quite strong. At
higher pressures, however, quenching can be a problem. The major disad-
vantage of this technique is that $BCl_3$ must be introduced into the dis-
charge to form the BCl radical. This has the potential to change the
characteristics of the discharge and produce distorted results.

## 2.3.3 Saturation Spectroscopy

Greater accuracy in electric-field measurements can be obtained if the individual fine-structure components can be measured. To fully realize the improvements in accuracy, one must utilize a Doppler-free technique. Saturation spectroscopy is one approach that could be considered for obtaining Doppler-free spectra.

Saturation spectroscopy is based on the saturation of a Doppler-broadened transition by optical pumping with a monochromatic tunable laser. The velocity distribution of the lower level is depleted by the monochromatic laser beam according to the resonance condition given in Eq. (7).

As a result of the depletion of the lower level, a "hole is burnt" in the velocity distribution as shown in Fig. 4. A counterpropagating beam would "burn a hole" in the distribution symmetrically displaced about $\omega_o$ since it would be in resonance with species Doppler shifted by $-\bar{k} \cdot \bar{v}$. Because of the "hole-burning" effect, the absorption of the transition is decreased at frequency $\omega$, and this forms the basis for saturated-absorption-spectroscopy techniques.

A monochromatic laser beam is split into two components—a strong pump beam and a weak probe beam—and the two components are passed counter-propagating through the sample. The two beams interact with different
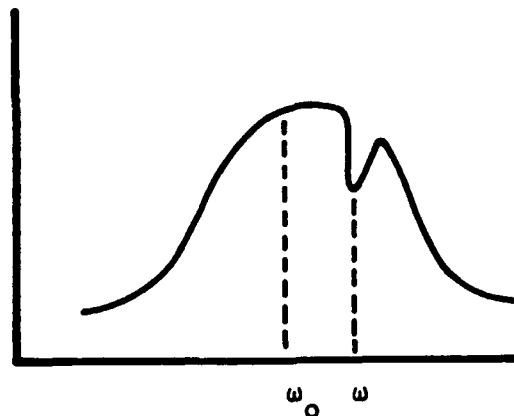


Figure 4. "Hole-Burning" of Lower-Level Population Distribution of Absorbing Transition.

12

velocity groups symmetrically distributed about $\omega_o$. However, at $\omega = \omega_o$, both beams interact with the same velocity group; i.e., those for which $\bar{k} \cdot \bar{v} = 0$. If the intensity of the probe beam is monitored, a decrease in absorption will be observed at this frequency because of the decrease in lower-level population caused by the strong pump beam. The width of this signal is independent of the Doppler width since it is generated by absorbers for which $\bar{k} \cdot \bar{v} = 0$.

The most common approaches for observing the dip utilize c.w. dye lasers with lock-in amplifiers to improve the signal-to-noise ratio. This approach would not meet our requirements regarding temporal resolution.

Hansch, et al.,[7] have developed a method for obtaining saturated absorption spectra with pulsed lasers. Their apparatus, as shown in Fig. 5, is not suitable for our application. The problem lies in the use of a reference and probe beam to enhance the signal-to-noise ratio. Since the plan is to probe regions of the discharge where the electric field varies strongly with distance, the probe and reference beams will interact with absorbers having different Stark components. The method could be used without a reference beam; however, the sensitivity would be much less. Consequently, saturated absorption spectroscopy is not felt to be a good approach.

## 2.3.4 Intermodulated Fluorescence Spectroscopy

In this Doppler-free technique, two counterpropagating laser beams are passed through the absorbing sample.[8] The two beams are modulated at frequencies $\omega_1$ and $\omega_2$. By detecting the fluorescence at the sum frequency, $\omega_1 + \omega_2$, one detects the Doppler-free signal only. Assuming that scattered laser light can be rejected, this approach is much more sensitive than saturated absorption spectroscopy. The technique has been used successfully to study the $2^3P - 3^3D$ isotope shift of He in a simple glow discharge[9] and has been most commonly used with c.w. dye lasers; however, one could use a high-frequency pulsed dye laser such as an excimer- or $N_2$-laser-pumped dye laser to obtain temporal resolution.
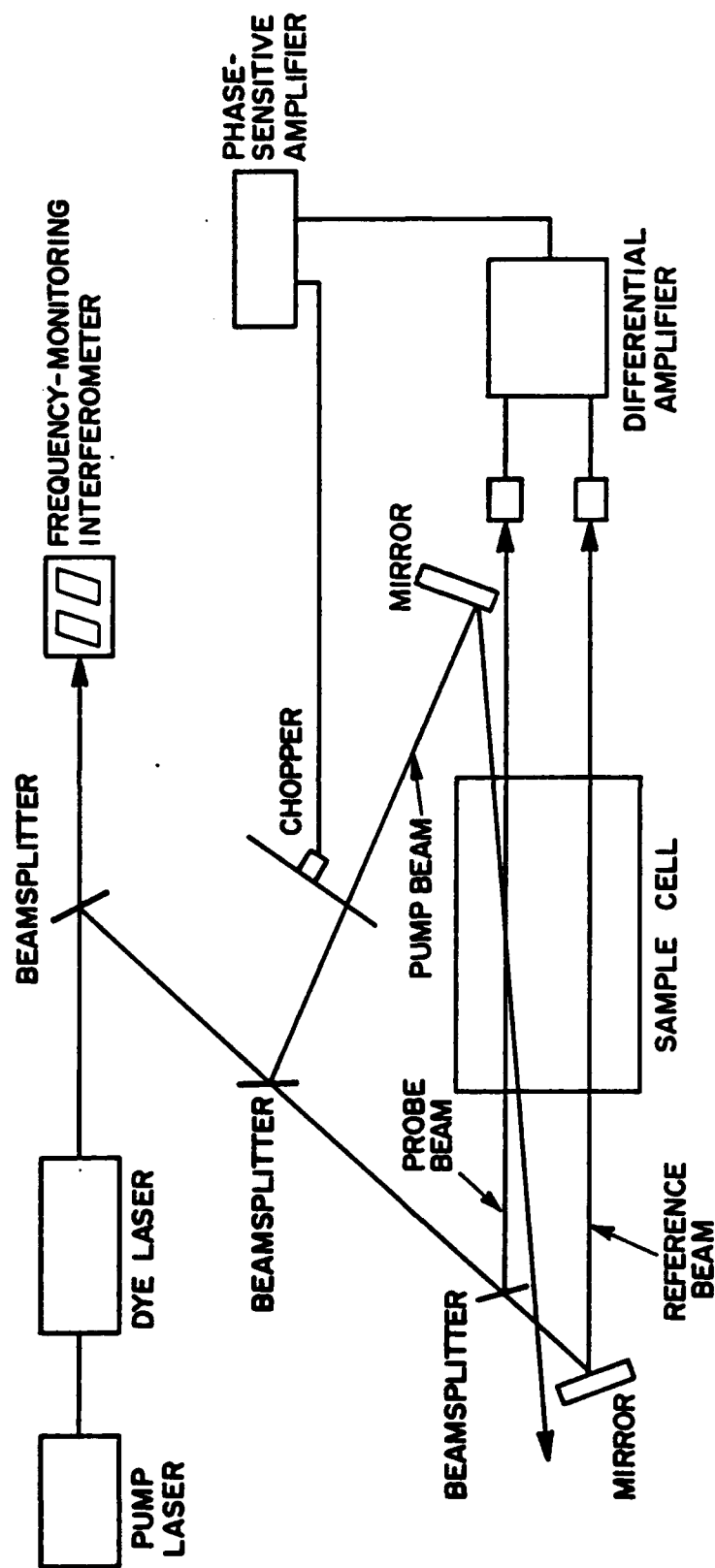
Figure 5. Pulsed Saturated Absorption Spectrometer.

The technique would not work well with 10-Hz Nd:YAG laser systems because the modulation frequencies would be too low for phase-sensitive detectors to be used. However, with appropriate equipment, this method would be viable. It offers good sensitivity and could potentially measure fields as low as 10 V/cm in an appropriate experiment.

2.3.5  Intermodulated Optogalvanic Spectroscopy[10]

This experiment is performed in the same fashion as the previously described one, with the following exception:  rather than observing the modulated fluorescence, one detects the change in the optogalvanic signal. The optogalvanic signal is the voltage change measured across the ballast resistor of the discharge when the impedance of the discharge is changed by optical pumping with a laser. This method of detecting an absorption process is quite sensitive and has an inherent advantage over fluorescence detection because it is not limited by scattered laser light. The major source of noise in this detection scheme is the noise in the discharge. Consequently, this technique is not useful in unstable or pulsed discharges. However, in stable D.C. discharges where scattered laser light is a problem, the optogalvanic technique would be very useful.

2.3.6  Optogalvanic Spectroscopy of Rydberg States

Doughty, et al.,[11] have shown that the highly sensitive optogalvanic effect can be employed to measure the linear Stark effect of Rydberg levels in He. The Rydberg states are very sensitive to external fields owing to the very large orbitals associated with these levels. The high sensitivity of the optogalvanic effect allows high Rydberg levels to be probed. This can result in a very sensitive probe of the electric field over a wide range. The drawback of this technique is the need for a relatively stable discharge for optimum detection. If this hurdle could be overcome, this technique would be a very useful probe of electric fields in most discharges.

15

## 2.3.7 Two-Photon Spectroscopy

It can be shown from the theory of nonlinear susceptibilities[12] that an absorbing medium can simultaneously interact with two photons at $\omega_1$ and $\omega_2$ if $\omega_1 + \omega_2$ is equal to a resonance of the absorber. In the special case where $\omega_1 = \omega_2$ and the two beams are counterpropagating, the signal will consist of sharp Doppler-free resonances on top of a Doppler-broadened profile.

A typical apparatus consists of a laser focused into the sample medium with a retroreflecting concave mirror to establish the counterpropagating beam.[13] The signal can be detected by observing the resulting fluorescence or by detecting the optogalvanic signal.

This experiment can be employed at wavelengths which are one-half the value of those produced by dye lasers. That is, pulsed dye lasers can produce light from 227 to 800 nm; consequently two-photon experiments can be performed from 113 to 400 nm. The advantage of working in this wavelength range is that one can access high n states where the Stark splitting is much larger than in lower-lying transitions without doubling the dye-laser output. In addition, laser scatter is much less of a problem because the signal can be monitored at the wavelength corresponding to an allowed one-photon transition, well removed from the excitation wavelength.

As a result of the recent conversations with Dr. Carl Wieman, a novel approach for detecting two-photon transitions should also be considered. This method is based on the selection rules for two-photon transitions. The $\ell$ selection rule is

$$\Delta \ell = 0, \pm 2 \tag{13}$$

In addition, there are selection rules for photon angular momentum (q). For $\sigma-$ (left-hand circularly polarized light), group theory gives $q = -1$; for $\sigma+$ (right-hand circularly polarized light), $q = +1$ and $q = 0$ for $\pi$ polarized light. The $m_\ell$ selection rule is

16

$$\Delta m_\ell = q_1 + q_2 \qquad\qquad (14)$$

A detection method for two-photon transitions could be devised in the following fashion. An intense $\sigma$-pump beam is passed through the medium. This beam is crossed by a counterpropagating weak probe beam of linear polarization. The linearly polarized beam is incident on a crossed polarizer which blocks it from a detector. The linear probe beam consists of·equal amounts of $\sigma+$ and $\sigma-$. If one wishes to pump an S-S transition [see Eq. (14)], then $\Delta m_\ell$ must be zero (since for S states $m_\ell$ is zero). Since the pump beam is $\sigma-$, to satisfy Eq. (14) only the $\sigma+$ component can be absorbed from the probe beam. This results in a rotation of the probe beam, and a signal would be detected through the crossed polarizer. Because the signal is coherent, there are two advantages of this technique over fluorescence detection. First, the entire signal can be collected, while in fluorescence only about 5% can be gathered. Second, the detector can be positioned remotely from the experiment in order to eliminate background radiation. In addition, the polarization method would be insensitive to collisional quenching.

The technique of Doppler-free two-photon spectroscopy is an excellent method and offers the possibility of resolution around 10 - 30 V/cm.

### 2.3.8 Microwave Spectroscopy[2]

Pure microwave spectroscopy is the classical approach to measuring molecular dipole moments. For discharges containing molecular species with permanent dipoles, microwave spectroscopy could be used as a very sensitive (10 V/cm) probe of electric fields.

Microwave spectroscopy has two important disadvantages. The first is that microwave selection rules require the species being detected to have a permanent dipole moment; therefore, many species of interest cannot be detected. Additionally, the Stark effect in species having no dipole moment is about $10^4$ times smaller than in those species possessing a dipole moment; therefore, only fields greater than $10^4$ V/cm can be detected. The second major difficulty with microwave techniques

17

is that radiation at these wavelengths cannot be focussed; consequently, spatial resolution cannot be obtained.

## 2.3.9 Microwave-Optical Double Resonance

A microwave-optical double-resonance pumping scheme is illustrated in Fig. 6. In this approach the microwave resonance is detected by observing an increase in laser-induced fluorescence arising when microwave excitation increases the population in the lower state. The major advantage of this approach is that spatial resolution is determined by the probing laser rather than the microwave source and, consequently, can be quite good. In addition, when species possessing permanent dipole moments are present in the discharge, the method is very sensitive to fields ( ~10 V/cm).

The technique experiences two major difficulties: 1)spectroscopic requirements are fairly restrictive since there must be species with both a permanent dipole moment and a fluorescence transition accessible by means of dye lasers, and 2) the experiment requires tuning two radiation sources to locate the Stark resonances. However, assuming that these two difficulties could be overcome, this technique is potentially an excellent one.
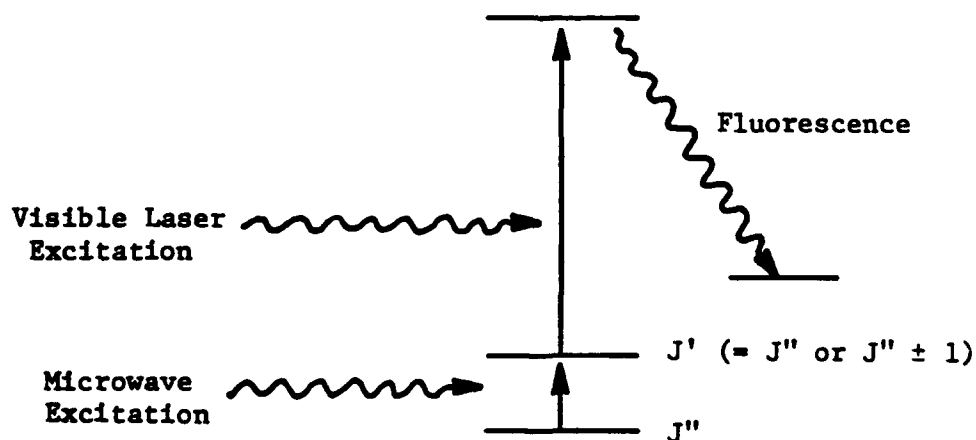
Figure 6. Microwave-Optical Double-Resonance Pumping Scheme.

## 2.3.10 Ultraviolet-Infrared Double Resonance

Recently Bloomfield, et al.,[14] demonstrated that, using a tunable dye laser and color-center I.R. laser, one can study Rydberg transitions in He with very high resolution. In their approach, a frequency-doubled laser was used to pump the $2^3S \rightarrow 5^3P$ He transition at 294.5 nm. A tunable color-center laser was then used to pump the $5^3P \rightarrow n^3D$ (n = 12-17) Rydberg transitions. The signal is detected by observing a decrease in the intensity of the U.V. fluorescence; therefore, the sensitivity of the technique should be independent of the large quenching cross sections of the Rydberg transitions. Additionally, since transitions with very high n are being studied, the sensitivity to fields should be excellent (10 V/cm).

Rydberg states typically have large pressure-broadening coefficients; however, from the data of Bloomfield, et al.,[14] the pressure-broadening coefficient can be estimated to be about 1.5 GHz/Torr (0.05 $cm^{-1}$/Torr). Consequently, the pressure-broadened linewidth should equal the Doppler width at about 30 Torr. At that linewidth, one could still resolve fields around 40 V/cm. At 1 atm., the resolution would degrade to 200 V/cm. This approach is a very viable method for studying electric-field distributions.

## 2.3.11 Polarization Spectroscopy

The technique of polarization[15,16] spectroscopy was developed specifically for Doppler-free studies of $H_\beta$ in glow discharges. Figure 7 shows the apparatus. A circularly polarized pump beam is passed through a sample. A second linearly polarized counterpropagating probe beam is also passed through the sample. The probe beam is blocked from the detector by a crossed polarizer. The linearly polarized probe beam may be viewed as being composed of two circularly polarized beams—one rotating in the same sense (+) and the other rotating in the opposite sense (-). In the absence of any optical anisotropy, the two components retain equal phase and amplitude passing through the medium and, therefore,
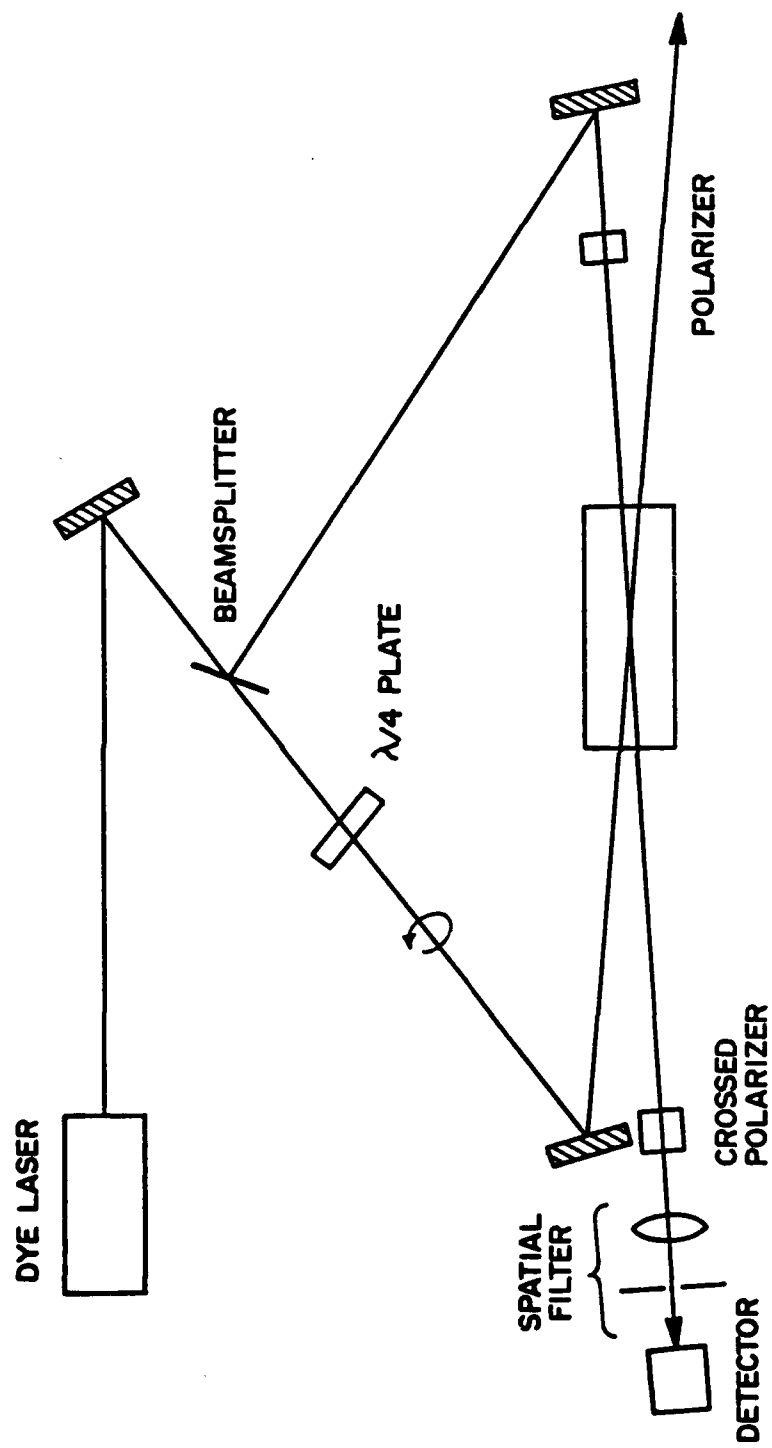
Figure 7. Polarization Spectrometer.

no signal is detected through the polarizer. In the presence of the pump beam, however, the medium is depleted of absorbers which interact with the + component. As a result, the absorption coefficient $\alpha_+$ no longer equals $\alpha_-$. This defines a circular dichroism which rotates the linearly polarized beam in such a way that a signal is detected through the polarizer.

Polarization spectroscopy is very sensitive. In direct comparison with intermodulated fluorescence spectroscopy, polarization spectroscopy was found to be 100 times more sensitive.[16] Additionally, fields as small as 10 V/cm could be measured using the $H_\beta$ transition.

## 2.3.12 Coherent Optical Transients

Several coherent-optical-transient techniques which have been examined are described below.

### Quantum-Beat Spectroscopy

When two (or more) upper levels are excited by the same laser source, the time-resolved total fluorescence intensity decays exponentially with a sinusoidal modulation. The modulation is referred to as quantum beats. It is due to interference between the fluorescence amplitudes of the coherently excited upper states. The beat frequency is related to the energy gap between the upper levels. In principle, one could use the beat frequency to determine Stark splitting; however, the upper levels must maintain coherence during the radiative-decay process for the beat to be detectable. Consequently, quantum beating could not be detected at normal discharge pressures, and this technique is not considered viable.

### Optical Nutation and Free-Induction Decay

When a two-level system is driven by an intense radiation field, the system alternately undergoes absorption ($E_1 \rightarrow E_2$) and stimulated emission ($E_2 \rightarrow E_1$). The system is alternatively driven between the

upper and lower states. The frequency at which the population oscil-
lates between the two levels is called the Rabi flopping frequency.
The flopping frequency is dependent upon the laser intensity and the
detuning of the laser from exact resonance. After a time, the Rabi
flopping is damped out and reaches a steady state; therefore, the
flopping can be observed only during the onset of the absorption
process. This flopping is the optical-nutation signal.

The free-induction decay arises when the coherently prepared system is
suddenly switched out of resonance with the driving field. The system
produces an oscillating dipole at some frequency now different from
that of the laser. This produces a beat frequency which is directly
proportional to the detuning of the transition from the laser.

Unlike quantum beating, optical nutation and free-induction decay can
be detected at high pressures and has been observed in flames.[17] An
experiment for measuring Stark fields in pulsed discharges could be
designed in the following fashion. An infrared laser could be tuned
to a specific molecular absorption (for example, $CO_2$). When a breakdown
voltage is applied, the species would be Stark shifted out of resonance,
and the nutation and free-induction decay signals would be generated.
By monitoring the frequencies of the oscillations, the fields could be
deduced. The spatial resolution of this approach would be limited to
line-of-sight and to the minimum unfocused diameter of the laser
( ∿ 0.5 mm); however, it would be a very elegant approach for measuring
fields in pulsed discharges.

## 2.3.13  Coherent Raman Techniques

A number of coherent Raman techniques such as CARS and stimulated Raman
gain spectroscopy have also been considered. CARS has been ruled out
because to obtain adequate spatial resolution, the signal-intensity
sacrifice is too great. Stimulated Raman gain spectroscopy has also
been eliminated because it lacks temporal resolution.

The five techniques considered to be most generally useful are rated in Table 2 according to the best assessment of the overall attainable field measurement accuracy (based on an estimate of the lowest field strength (measurable), experimental difficulty, and detection sensitivity (i.e., relative signal-to-noise considerations). Note that these rankings are necessarily qualitative and can vary widely for a given set of discharge conditions with a given set of available spectroscopic transitions. The rankings are determined by assuming optimum conditions.

## 2.4 Technique Selection and Limitations

The first step in choosing a technique is to decide on the discharge of interest. There are a large number of potential discharge media; however, this discussion will be restricted to H and He. This choice is based on the fact that the spectroscopy of these two species is well understood. Additionally, the Stark effects can be accurately predicted from quantum mechanics; and, consequently, no calibration methods will be required.

TABLE 2

RANKINGS OF THE FIVE BEST TECHNIQUES

1. Field Measurement Accuracy

    Optogalvanic Spectroscopy ≈ Polarization
    Spectroscopy ≈ Microwave-Optical Double Resonance
    > Two-Photon Spectroscopy ≈ Infrared-Optical
    Double Resonance

2. Experimental Difficulty

    Two-Photon > Optogalvanic Spectroscopy
    > Polarization Spectroscopy > Microwave-Optical Double
    Resonance ≈ Infrared-Optical Double Resonance

3. Detection Sensitivity

    Polarization Spectroscopy ≥ Optogalvanic Spectroscopy
    > Microwave-Optical Double Resonance ≈ Infrared-Optical
    Double Resonance > Two-Photon Spectroscopy

23

For H, the most accurate method is believed to be polarization
spectroscopy. This method has been demonstrated[15] to yield very
accurate measurements of fields in the positive column of a simple glow.
Based upon the linewidth of our laser (150 MHz), a lower limit to
field measurements of 10 V/cm is anticipated if the $H_\beta$ transition is
used. If sensitivity is a problem, $H_\alpha$ can be employed.

The absorption coefficient for $H_\alpha$ is about ten times greater than for
$H_\beta$; however, the Stark splitting in $H_\alpha$ is less and, therefore, the
lower limit would be raised to 20 V/cm. Although polarization spectros-
copy has not been demonstrated at high pressure, after discussing this
question with Dr. Carl Wieman, it is believed there is no physical reason
why the experiment cannot be performed at 1 atm.

For He discharges, it is proposed to use two-photon spectroscopy since
in order to obtain low-field measurements, one must use high-n quantum-
number transitions. It is estimated that the minimum field measurement
which could be obtained using the $2^1S - 8^1D$ transition is 30 V/cm. To
ensure a stable discharge, a hollow-cathode system will be employed.
This will ensure maximum sensitivity with minimum noise from the dis-
charge.

The temporal resolution for both experiments is about 15 nsec. (the
duration of the laser pulse). The line-of-sight spatial resolution of
H polarization spectroscopy will be limited by the minimum interaction
length of the two crossing beams required to obtain adequate signals.
The minimum length will be determined experimentally by the number
density of H atoms but will be on the order of several centimeters.
The spatial resolution determined by the beam diameter is anticipated to
be on the order of 100 μm. The spatial resolution for optogalvanic
spectroscopy is limited to a line of sight. However, multi-step or two-
photon excitation can potentially be used to solve this problem.

For the pulsed discharge studies, the LIF signal of the BCl radical was
chosen due to its high sensitivity to the applied field and its demon-
strated ability to work in varying electric fields.

24

The major anticipated limitation on field measurements will arise from line broadening due to collisions with electrons and neutrals.

The collisional pressure-broadening coefficients for $H_\beta$ and the $2^3S - 8^3D$ He transition are not available in the literature. The pressure-broadening coefficient for $H_\alpha$ by He is 75 MHz/Torr. In the present work the broadening coefficient for $H_\beta$ has been estimated to be 100 MHz. For He, 500 MHz/Torr has been assumed to be reasonable for a Rydberg state. Using these numbers Fig. 8 has been constructed which shows the minimum measureable field as a function of pressure. In constructing this diagram, the Stark effects were calculated for $H_\beta$ by diagonalizing the perturbation matrix. For He, the Stark splitting was estimated using Eq. (4) and Table 1. Above 50 Torr, the assumption was made that it was no longer necessary to resolve the individual Stark components in order to determine the field accurately. The lower detectable field was determined by first calculating the pressure broadening and then calculating the Stark broadening required to increase the linewidth 25% (a conservative number).

A major difficulty arises from the role played by electron collisions. Electron collisions introduce a linewidth from both elastic and inelastic scattering. The elastic cross section is about 25 $Å^2$ at 1 eV. From Eq. (12), this introduces a line broadening equal to $2.1 \times 10^{-7}$ $N_e$.

This is less than our laser linewidth of 150 MHz for electron densities less than $7 \times 10^{14}$ $cm^{-3}$. Elastic cross sections are somewhat larger, being equal to 35 $Å^2$ at 10 eV.

The electron-collision cross sections are not that much greater than the neutral cross sections and, assuming less than 0.1% dissociation, will make only a minor contribution. More important, however, is Stark broadening from electron microfields. An electron or ion near an emitter will produce a local electric field which is characteristic of the environment of the emitter but is different from the true electric-field distribution. The microfield can be related to the electron density through the normal field-distribution function given by
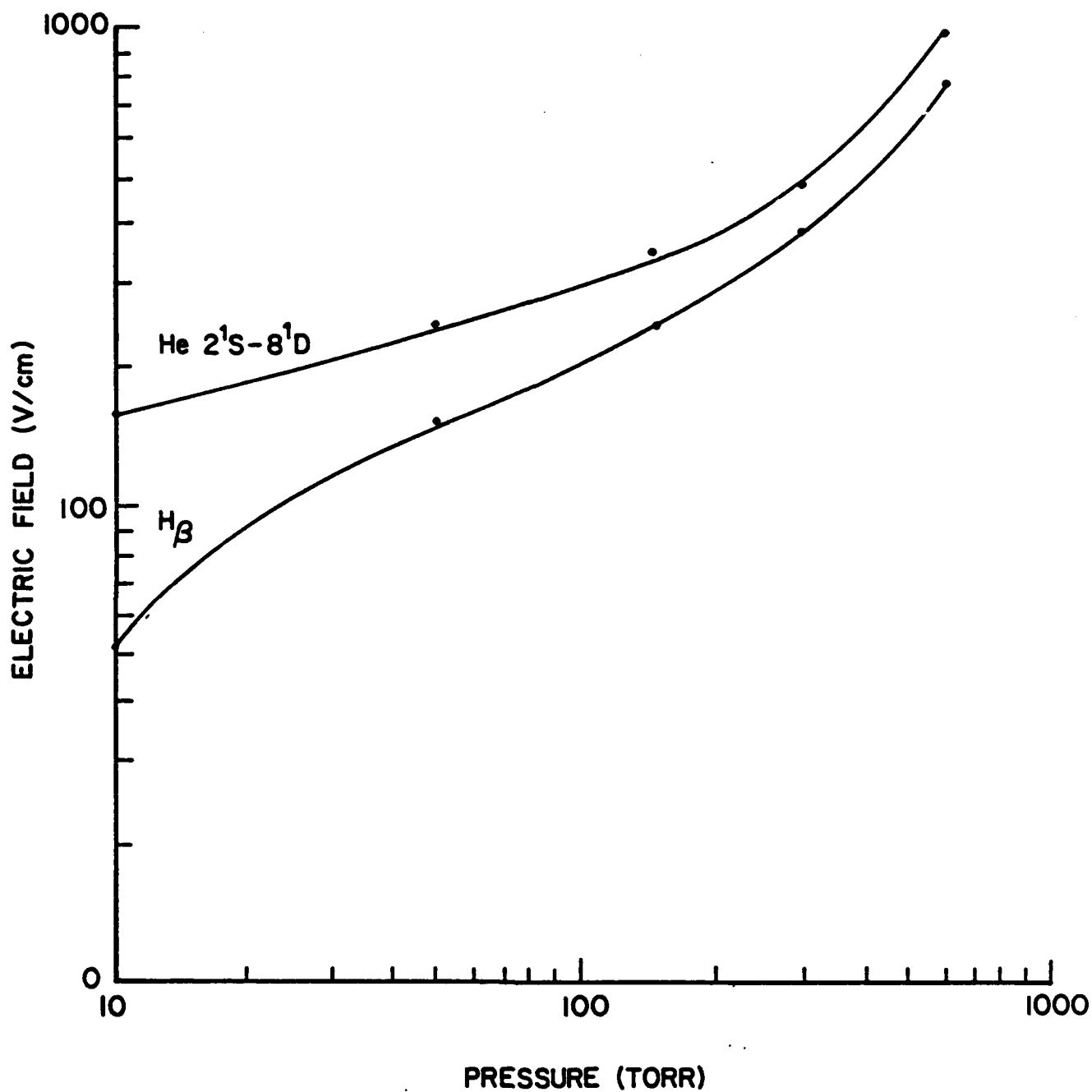
Figure 8.  Plot of Lowest Measurable Electric Field as Function
of Pressure.

$$F_o = 3.75 \times 10^{-7} (N_e)^{2/3} \tag{15}$$

where $F_o$ is the normal field (V/cm) and $N_e$ is the electron density.
For an electron density of $10^{14}$ cm$^{-3}$, this produces a field of 800 V/cm.
If the Stark broadening from the microfield is taken as the lower limit
for measuring the electric fields, then one can estimate the lower field
measurement for a given electron density from Eq. (15). This can pose
a serious limitation. For example, at $10^{17}$ cm$^{-3}$, the microfield is
equivalent to $7 \times 10^{4}$ V/cm.

In conclusion, the limitations on the lowest measureable fields are, for
low $N_e$, determined by neutral broadening and can be determined from
Fig. 8. For high $N_e$ relative to neutral broadening, the lower limit is
set by the microfield and can be calculated from Eq. (15). These limita-
tions are significant; however, the techniques presented here will allow
data to be obtained over a wide range of discharge conditions.

## Section 3
## EXPERIMENTAL ASSESSMENT OF TECHNIQUES

### 3.1 Polarization Spectroscopy

In the theoretical-assessment section, important experimental considerations were identified for observing Stark effects in hydrogen. Because of the large Doppler width of hydrogen (0.27 $cm^{-1}$ at 300 K), measurements of the Stark effect require a Doppler-free spectroscopic technique at low fields (< 1,000 kV/cm). Of the available methods, laser polarization spectroscopy is considered to be the best technique for hydrogen atoms. Figure 7 shows the experimental arrangement employed in these studies. The circularly polarized pump beam depletes the sample of atoms oriented to absorb light of one circular polarization, leaving an excess of atoms in the lower level with the opposite sense of polarization. The linearly polarized probe beam can be viewed as being composed of two circularly polarized waves of equal intensity, rotating in opposite directions. Since the ground state acquired an excess of atoms having one particular polarization resulting from the saturating beam, one component of the linearly polarized beam is preferentially absorbed. This results in a rotation of the probe beam in such a way that a signal is transmitted through the crossed polarizer. Since the probe and pump beams are counter-propagating, the technique is Doppler-free. Additionally, the technique has a signal-to-background noise ratio under ideal conditions which is 100 to 1,000 times higher than that of saturated absorption spectroscopy.[15]

The residual Doppler width of the transition is given by

$$\Delta \nu = \frac{0.6 \; \theta}{2 \pi} \; \Delta \nu_d \tag{16}$$

where $\theta$ is the crossing angle of the two beams in radians and $\Delta \nu_d$, the Doppler width. For $\theta = 1$, the residual width is 2 MHz; therefore, it is clear that the beams must be nearly collinear.

Since high spatial resolution is desired, the effects of transit-time broadening upon linewidth have been considered. Transit-time broadening arises from atoms moving out of the excitation region and is given by

$$\Delta \nu = \frac{0.58}{2\pi} \frac{v}{r} \tag{17}$$

where v is the atomic velocity and r the beam diameter. For atomic hydrogen at room temperature in a beam of 0.1 mm diam., the transit-time broadening is 2 MHz.

The collisional linewidths of the Balmer-$\beta$ transition are not yet known, but broadening of the Balmer-$\alpha$ line is 75 MHz/Torr[2] for helium as the collision partner.[18] It can be estimated that for the Balmer-$\beta$ line in $H_2$, collisional linewidths will be $\sim$ 100 MHz/Torr. Consequently, the low-field experiments were performed at a pressure around 0.1 Torr.

Initial demonstrations of the polarization setup were made on the He 501.57-nm line. The He 501.57-nm transition was chosen because of the relative ease with which the $2n^1S$ He metastable can be produced. With a current of only 5 mA, 85% absorbance could be obtained. To obtain a correct value for absorbance, however, care was taken to avoid saturation. For the 501.57-nm transition, saturation was observed above 3 W peak laser power. Figure 9 shows a typical absorption spectrum. To obtain a polarization spectrum, the probe beam was attenuated in such a way that it was below the saturation level. Also, the pump beam must be attenuated to avoid power broadening. Figure 10 shows a typical polarization spectrum. The laser linewidth is the same as in Fig. 9, but the spectrum is Doppler-free; therefore, the linewidth is reduced to that of the laser, i.e., 0.03 $cm^{-1}$.

Additionally, results with $H_\alpha$ have been obtained. For achieving adequate concentrations of H atoms, the tube was coated with orthophosphate acid and the discharge operated as a mixture of He and $H_2$. Maximum $H_\alpha$ absorption was obtained with a $H_2$ pressure around 0.1 Torr. Higher pressure reduced the absorption signal. When the discharge was operated in this fashion, the positive column was bright red with no striations.
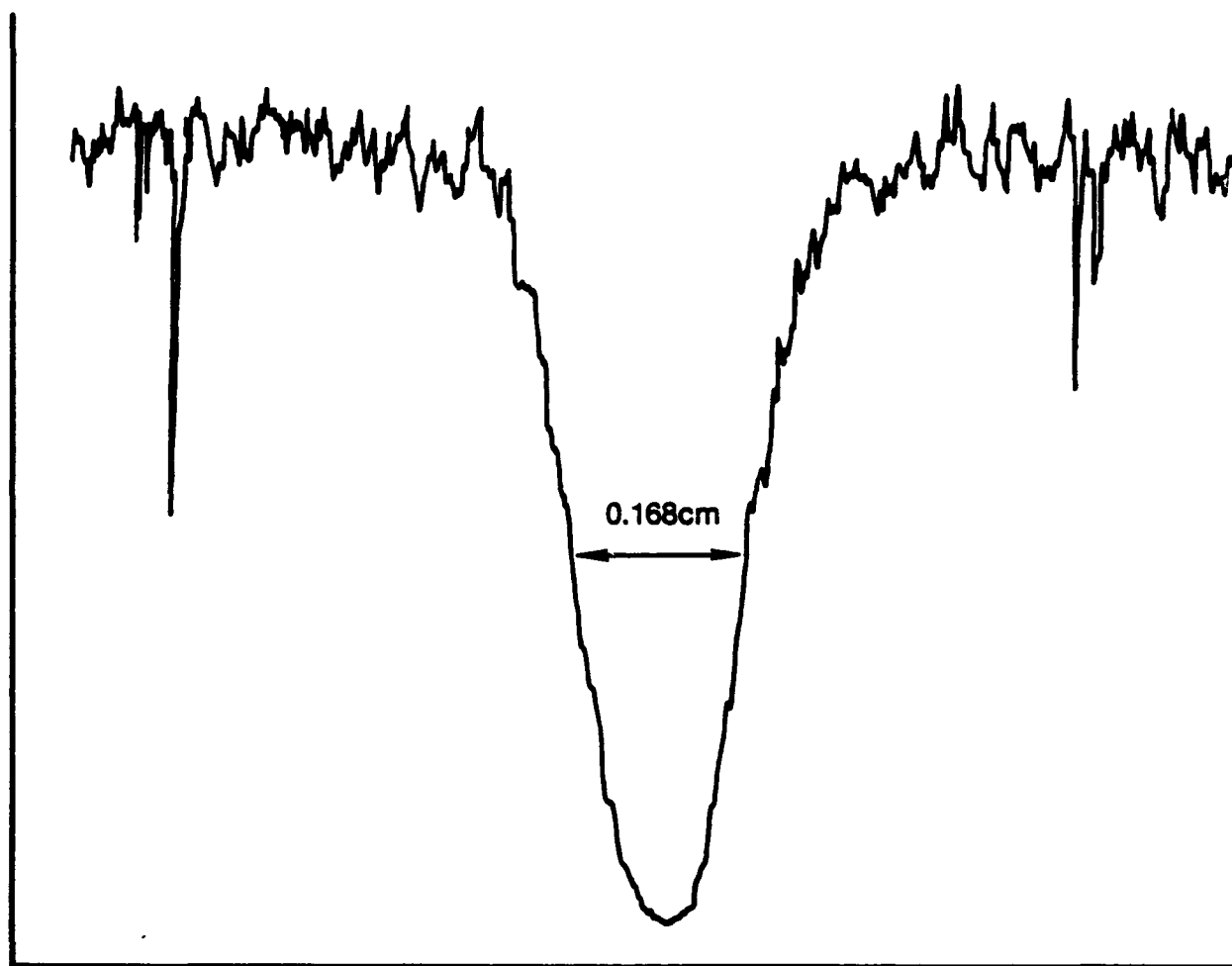
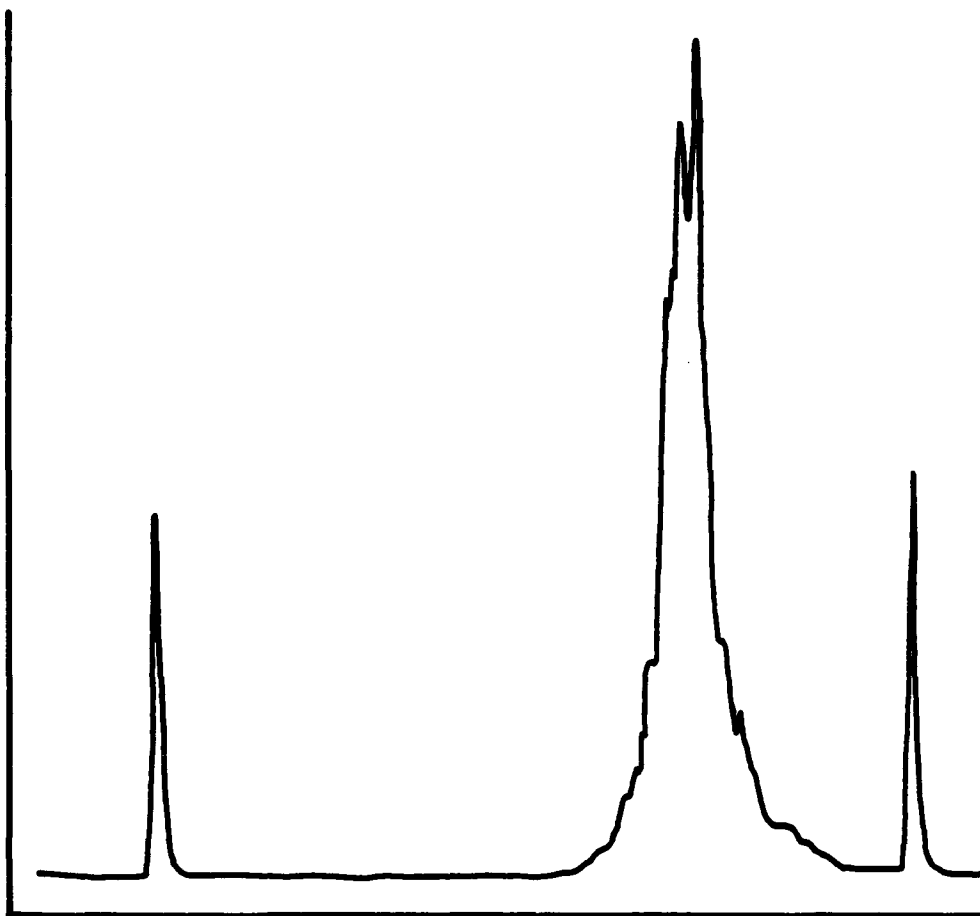Figure 9. Absorption Spectrum of 501.5-nm Transition.

Figure 10. Doppler-Free Polarization Spectrum of He 501.5-nm
Transition. Linewidth is 0.03 cm$^{-1}$.

Figures 11 and 12 display the absorption and polarization spectra of $H_\alpha$,
respectively.

$H_\beta$ was expected to be a more difficult example because of its six-times-
lower oscillator strength. Figure 13 shows a Doppler-free polarization
spectrum of $H_\beta$. This spectrum was taken with the maximum dye-laser
resolution by means of the 150-MHz-bandwidth external interferometer.
At this resolution the $^2S_{1/2} - {}^4P_{1/2}$, $^2S_{1/2} - {}^4P_{3/2}$, and $^2P_{1/2} - {}^4D_{3/2}$
transitions should have been resolved in the spectrum. Line-broadening
effects such as collisional broadening and electron broadening have been
ruled out. Later, it was determined that the glass windows of the dis-
charge cell were heating up, causing a change in the birefringence which
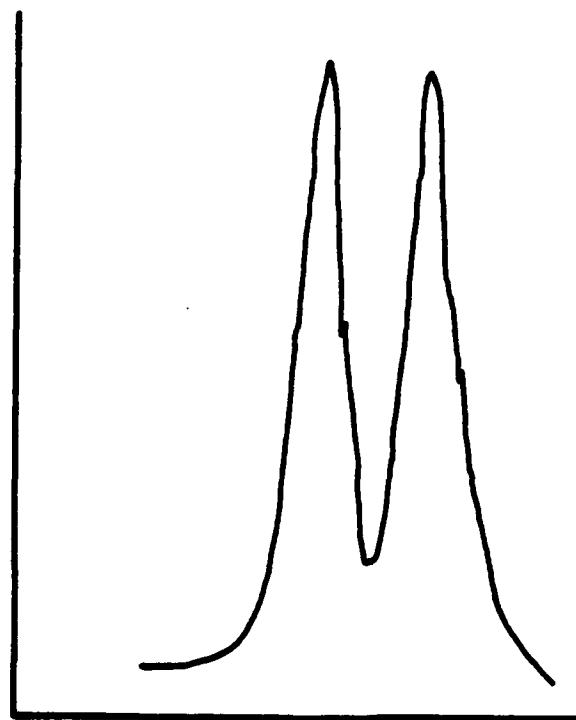
Figure 11.   Absorption Spectrum of $H_\alpha$.



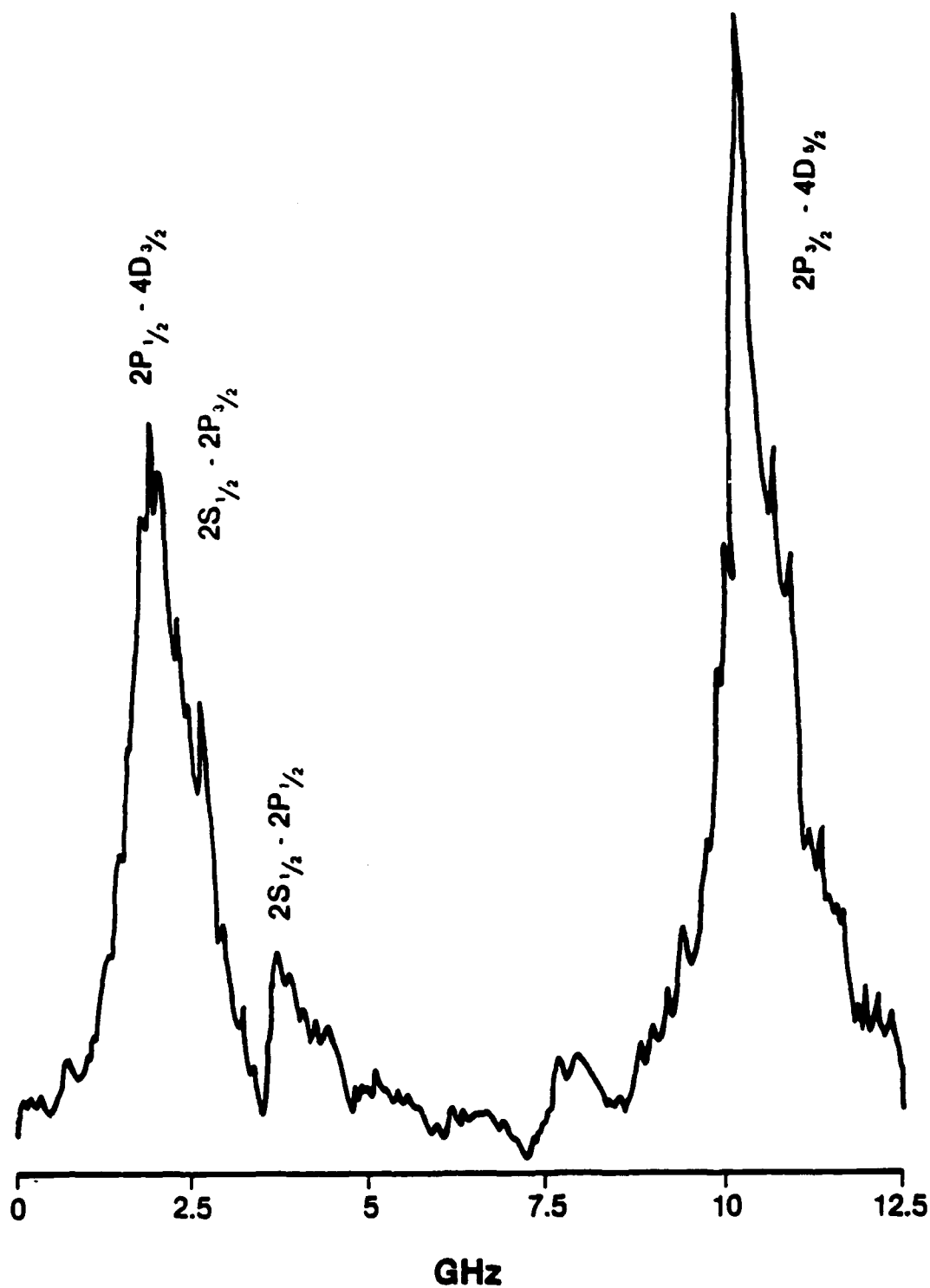Figure 12.   Doppler-Free Polarization Spectrum of $H_\alpha$.

Figure 13. Polarization Spectrum of $H_\beta$.

resulted in a degraded signal-to-noise ratio. By replacing the glass windows with quartz, this ratio improved dramatically which, in turn, allowed the power of the laser probes to be reduced. This is important because of the power-broadening problem.

The linewidth of a homogeneously broadened spectral transition pumped by a laser is given by

$$\Delta\nu = \Delta\nu_o (1 + S)^{1/2} \tag{18}$$

where $\Delta\nu_o$ is the homogeneous linewidth in the absence of a laser field and S the saturation parameter given by

$$S = \frac{B\rho(w)}{R} \tag{19}$$

Here B is the Einstein coefficient, $\rho(w)$ the radiant-energy density (erg/cm$^3$), and R the relaxation rate of the upper level. Consequently, one must be able to obtain spectra using sufficiently small values of $\rho(w)$ that S will be < 1, which will eliminate power broadening.

Calibration of the dye-laser linewidth was made by taking the Doppler-free spectrum of isotopically pure Te 130. The Doppler-free polarization spectrum indicated that the dye-laser linewidth was ∿ 200 MHz and would allow the measurement of Stark shifts in atomic hydrogen. Thus, the main contribution to the observed broadening of the $H_\beta$ transitions was power broadening.

By reducing the probe-beam power to a minimum, the $H_\beta$ spectra shown in Fig. 14 were obtained. As the laser probes a region nearer the tube wall, it is observed that both the $^2S_{1/2} - {}^4P_{3/2}$ and $^2S_{1/2} - {}^4D_{3/2}$ transitions are shifted to lower energy. In addition, both the $^2P_{1/2} - {}^4D_{3/2}$ and $^2P_{3/2} - {}^4D_{5/2}$ transitions exhibit large amounts of broadening.
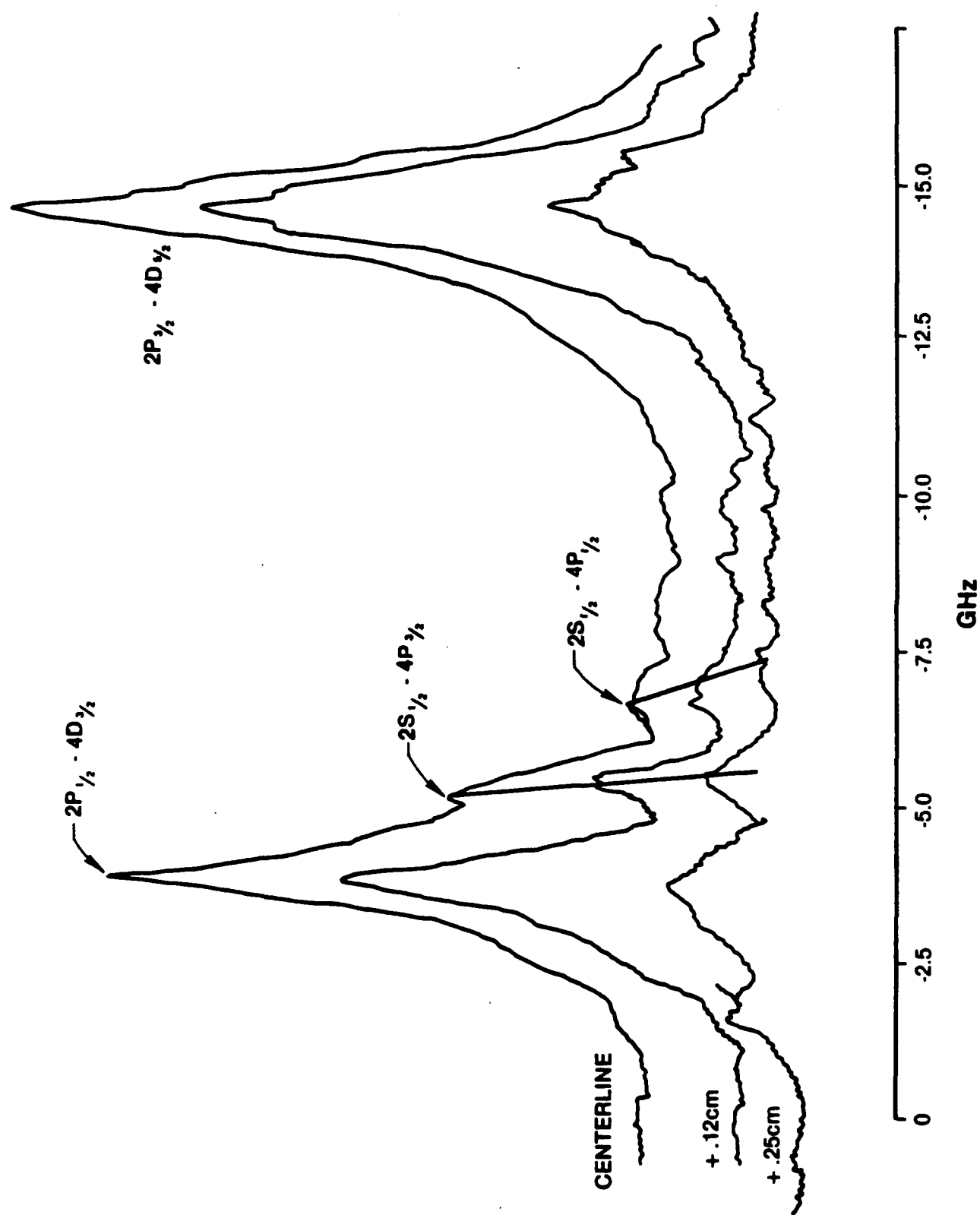
Figure 14. $H_\beta$ as Function of Position in Plasma Tube.

According to our previous Stark-effect calculations, these are the characteristics expected when the electric field increases. From the movement of the $^2S_{1/2}$ – $^4P_{1/2}$ transitions, the electric field was estimated to have increased by $\sim$ 17 V at 0.25 cm from the centerline.

As demonstrated by Fig. 14, the $H_\beta$ spectrum is significantly broadened, even at the lowest powers. Attempts to further reduce the probe power were not successful. The problem is that the high peak power of the pulsed dye laser broadens the spectrum well above the detection threshold. The technique is better suited to a cw than a pulsed probe beam. Because of this problem, the alternative approach to the low-pressure plasmas was taken.

3.2 Optogalvanic Spectroscopy of Rydberg States

This section reports the measurement of the electric-field profile in the cathode-sheath region of a hollow-cathode He discharge. Optogalvanic spectroscopy of Rydberg states of singlet He was chosen as the diagnostic method because of the sensitivity of the optogalvanic technique for examining states of relatively low population and strong sensitivity to electric fields. Both Stark splitting and allowed/forbidden intensity ratio methods were used to determine the electric field in the cathode-sheath region which varied from 1800 to 200 V/cm.

In an electric field the normal components of a spectrum are split by the Stark effect. The electric field induces a dipole moment in the atomic or molecular species. The interaction between the dipole and the field causes a precession of J, the angular momentum vector, about the applied field such that the $m_j$ components are a constant of motion. A change in direction of rotation of J has no effect upon the magnitude of the dipole; thus, the energy shifts for $+ m_j$ and $- m_j$ are the same. The value of the Stark shift can be deduced from quantum-mechanical calculations by constructing the perturbation Hamiltonian matrix using the perturbation operator eFz, where e is the electronic charge, F the field strength, and z the coordinate of the atom in the field. This was demonstrated for He by Foster.[5] Results of such calculations for the

36

Rydberg states of singlet He indicate that they are strongly affected by
the electric field and would, thus, provide a sensitive measure of the
field strength. The primary reason for the high sensitivity of the
Rydberg states to the electric field is the very large orbit of the out-
ermost electron of these states which makes them susceptible to perturb-
ing forces. By monitoring the Stark shifts of various Rydberg states of
singlet He, a wide range of electric fields can be measured.

Not only do the Stark components shift under the action of an electric
field, but a breakdown in transition selection rules can occur. Pertur-
bation theory[3] shows that in a weak electric field, a wave function
$\psi_{n,\ell,m}$ becomes mixed with the wave function $\psi_{n,\ell+1,m}$ resulting in a weak
transition for which $\Delta\ell = 0, \pm 2$ is observed. The intensity of the for-
bidden transition $J_1'$ from a level $n,\ell$ to $n_o,\ell$ is given by[3]

$$J'^{n_o,\ell}_{n,\ell} = \frac{9}{4} \frac{f^2}{(E_{n,\ell+1} - E_{n,\ell})^2} [n^2 - (\ell+1)^2]n^2 \frac{(\ell+1)^2 - m^3}{4(\ell+1)^2 - 1} J^{n_o,\ell}_{n,\ell+1} \quad (20)$$

where $J^{n_o,\ell}_{n,\ell+1}$ is the total intensity for an allowed transition $n,\ell+1$, $m$
to $n_o,\ell$, $m_o$ summed over all of $m_o$, and F is the electric field. Accord-
ing to Eq. (20) the allowed-forbidden intensity ratio of relatively high
Rydberg states would be quite sensitive to an applied electric field as
would an energy level in which the energy-level difference between the
allowed and forbidden transitions is small. Thus, as with line shifts,
the allowed/forbidden intensity ratio should show good sensitivity to
electric field.

The optogalvanic technique was chosen for this study because of its high
sensitivity for sparsely populated states. A change in the discharge
current or impedance is monitored by capacitively coupling to the dis-
charge. Rydberg states are easily observed in this manner because, once
formed, they are efficiently ionized by ion or neutral impact.[19]

The experimental arrangement employed for the optogalvanic experiments
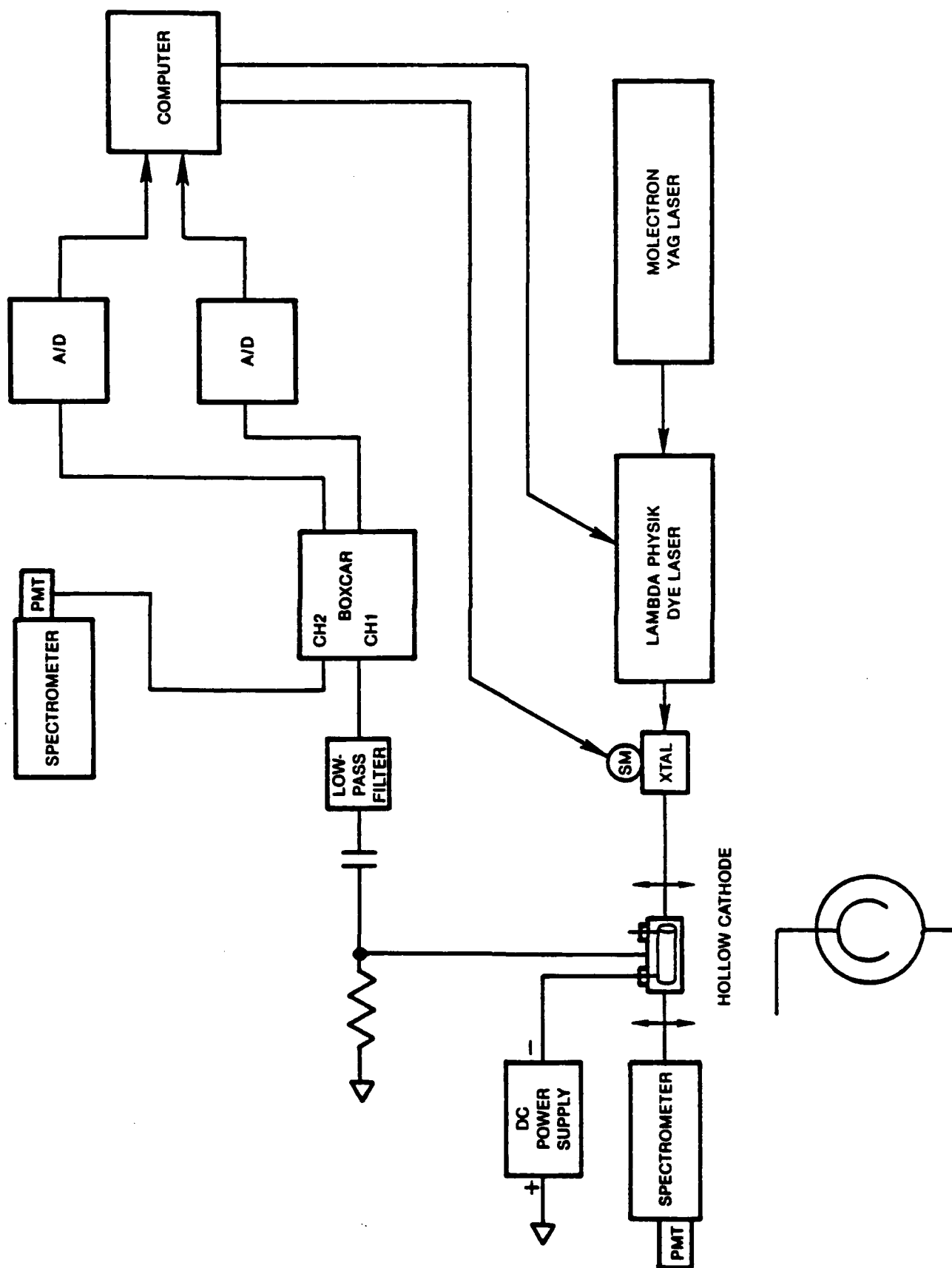is shown in Fig. 15. The frequency-doubled output from a Molectron

Figure 15. Experimental Arrangement Employed for Optogalvanic Experiments.

Nd:YAG laser was used to pump a Lambda Physik dye laser (0.2 cm$^{-1}$ FWHM linewidth). DCM dye was employed for lasing at $\sim$ 641 nm. The output of the dye laser was frequency doubled by a KDP crystal to generate $\sim$ 320 nm radiation for excitation of the $2s^1S$ - $11s^1P$ transition of He (0.4 cm$^{-1}$ FWHM). The polarization of the laser was maintained perpendicular to the electric field. A 30-cm focal-length lens was used to focus the frequency-doubled dye output in the center of a slotted-hollow-cathode discharge. The beam waist was $\sim$ 100 $\mu$ at focus but was as large as 300 $\mu$ at each end of the discharge tube. The unabsorbed light was passed through the discharge cell and monitored by a monochromator-PMT combination and an etalon with a 1 cm$^{-1}$ free spectral range. The unabsorbed beam was used to monitor shot-to-shot fluctuations as well as to tune the frequency-doubling crystal.

The optogalvanic signal was capacitively coupled and passed through a high-bandpass filter to eliminate low-frequency current fluctuations of the discharge and power supply. The filtered optogalvanic signal and the reference signal were fed into a BOXCAR integrator, the output of which was digitized and stored in a Digital 11/23 microcomputer. The optogalvanic signal was then normalized to the reference signal to account for pulse-to-pulse laser fluctuations and long-term drifts in the tuning of the frequency-doubling crystal.

A slotted-hollow-cathode discharge,[20] consisting of a tubular cathode slotted lengthwise and surrounded by a coaxial anode, was chosen for this study. The discharge tube was comprised of a 10-cm-long × 9.5-mm-o.d. Kovar cathode within a 19-mm-o.d. stainless-steel anode. The transverse discharge established between anode and cathode is characterized by an intense negative glow within the hollow cathode. The main discharge current is from the negative-glow plasma through the slot to the anode. The intense emission, low noise, and positive dynamic impedance make this an excellent discharge configuration for spectroscopic measurements.

Recent optogalvanic experiments on sparsely populated Rydberg states of He have demonstrated the high sensitivity of these states to an applied

electric field.[21-24]  Because of this sensitivity, electric-field pro-
files of glow discharges are now possible.  To demonstrate this fact, a
measurement of the radial profile of the electric field in a slotted-
hollow-cathode discharge was undertaken.  The discharge conditions were
2 Torr He, 50 mA, and 300 V.  The inner radius of the cathode was
3.6 mm.

To cover the entire electric-field range of interest, more than one
Rydberg state had to be examined.  Both line shifts (linear Stark
effect) and line intensities (allowed/forbidden) were employed in these
experiments to cover a variation in electric field from 1800 to
200 V/cm.  The singlet transitions $2s^1S - 11s^1P$, $2s^1S - 14s^1P$, and
$2s^1S - 17s^1P$ were employed in the 1800 to 1000 V/cm, 1200 to 400 V/cm,
and 400 to 200 V/cm ranges, respectively.  The experiment consisted of
optically pumping the He atom in the $2s^1S$ state to an upper Rydberg
state which was readily ionized, causing a small change in the impedance
of the discharge tube.  The net current change was then monitored, fil-
tered, and digitized for data analysis.  Based upon the observed spectra
of the probed transition, line shifts or forbidden-allowed intensity
ratios were measured for electric-field determination.  Figure 16 dis-
plays an experimentally observed $2s^1S - 11s^1P$ transition of He at a
field of 1575 V/cm.  The vertical lines in the figure depict the calcu-
lated location of the various Stark components.

A least-squares program was used to fit the line spacing as a function
of the electric field.  The experimentally measured results are shown in
Fig. 17 where the electric field versus distance from the cathode is
plotted.  Notice that at the cathode surface the field is quite high,
1800 V/cm, and drops off almost linearly with increasing distance from
the cathode, displaying some curvature at large distances.  By using
both line shifts and intensity data from multiple Rydberg levels, a
self-consistent check can be made of the measured fields.

The uncertainty in the spatial position of the measurements shown in
Fig. 16 is ± 50 μ owing to the beam profile of the probe laser.  The
uncertainty in the field measurement in the case of line splitting was
determined to be ± 75 V/cm, based upon the fit of the calculated line
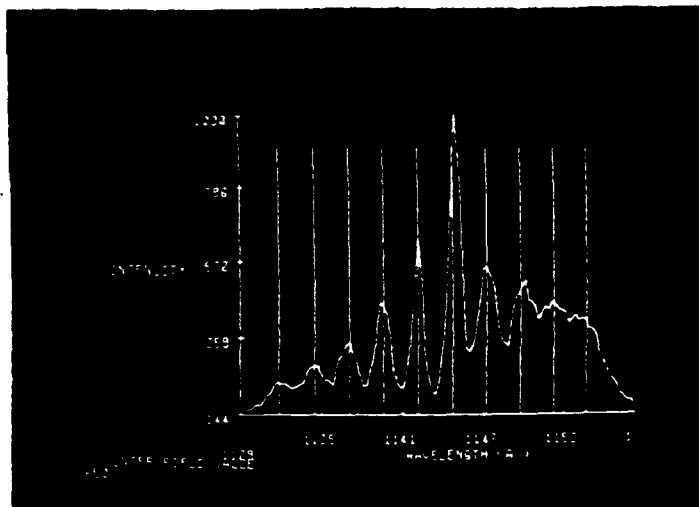
Figure 16.  Stark Spectrum Observed 0.3 mm
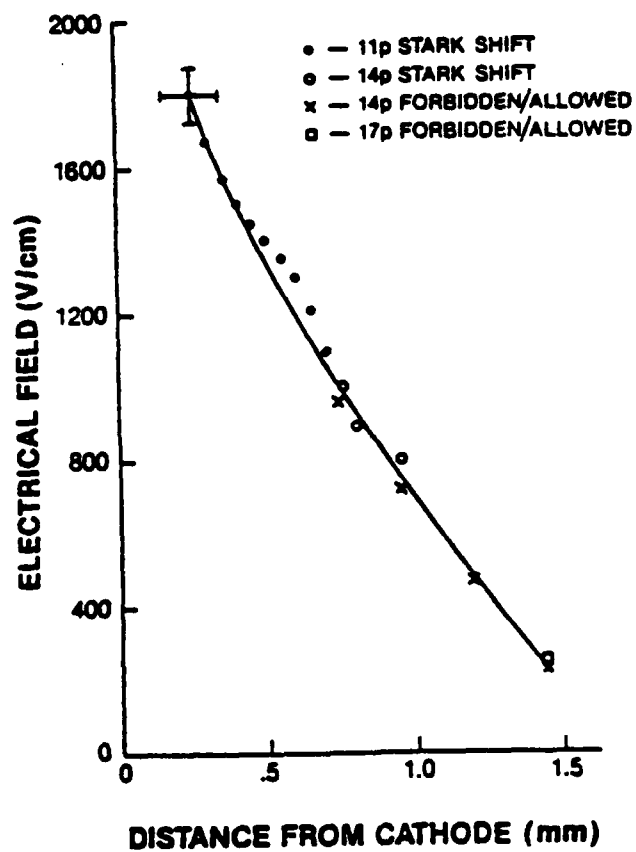from Cathode; E = 1575 V/cm.



DISTANCE FROM CATHODE (mm)

Figure 17.  Dependence of Electric Field
upon Distance from Cathode.

shifts to the experimentally observed line shifts. The uncertainty in the forbidden intensity measurement was determined by the signal-to-noise ratio of the observed optogalvanic signals. An uncertainty comparable to the line-shift measurements was observed in this study (± 50 V/cm).

The results of this study indicate that optogalvanic detection of Rydberg states of He allows a spatially resolved measure of the electric field in the cathode-fall region. Extensions of this technique to the study of high-pressure glow and pulsed discharges is presently being pursued.

### 3.3 Laser-Induced Fluorescence of BCl

Moore, et al.,[6] reported a sensitive, nonintrusive method of measuring electric fields by monitoring the field-induced mixing between diatomic rotational energy levels of opposite parity. The mixing manifests itself by the appearance of fluorescent lines which are forbidden in the absence of an external field. A case in point is the BCl radical which has a $^1\Pi \leftarrow {}^1\Sigma^+$ band system. In the absence of an external field, the electric-dipole allowed transitions change parity from +/- to -/+ and the rotational quantum number by 0 or +/-1. This implies that for R- and P-branch excitations ($\Delta J = 1$ and $-1$, respectively), only e levels are populated in the $^1\Pi$ excited state and only R- and P-branch lines are seen in fluorescence; for Q-branch excitation ($\Delta J = 0$), only f levels are populated and only Q branches are seen in fluorescence. However, in the presence of an external field, the e and f levels are mixed by the Stark operator whose matrix elements are given by

$$V(J < M) = \langle e,J,M | \mu \cdot F | M,J,f \rangle$$

$$= \frac{\mu F M}{J(J + 1)} \tag{21}$$

42

where M is the projection of J onto the electric field F and μ is the molecular dipole moment operator. The result is a sharing of oscillator strength between e and f levels and the appearance of forbidden lines.

The extent of mixing and, hence, the forbidden-line intensity, depends not only upon the interaction strength but also upon the zero-field e-f energy splitting (Λ doubling), Δ, which is quadratic in J: $\Delta = qJ(J + 1)$ where q is the Λ-doubling constant. The relative intensities of forbidden and allowed transitions are also a function of polarization. After transformation to the rotating molecule frame of reference, relative Q- and P-branch intensities as a function of electric field and fluorescence polarization are obtained for the case of z-polarized (laser polarized parallel to the plasma field) R-branch excitation and Λ doubling smaller than the laser bandwidth:

$$I_Q^g = \sum_m \frac{m^2[(J + 1)^2 - m^2]}{(J + 1)^2(2J + 1)(2J + 3)} \frac{\phi^2}{1 + \phi^2} \tag{22a}$$

$$I_P^g = \sum_m \frac{[(J + 1)^2 - m^2][(J + 2)^2 - m^2]}{(2J + 1)(2J + 3)^2(2J + 5)} \frac{2 + \phi^2}{1 + \phi^2} \tag{22b}$$

$$I_Q^x = \sum_m \frac{[(J + 1)^2 - m^2][(J + 1)(J + 2) - m^2]}{2(J + 1)^2(2J + 1)(2J + 3)} \frac{\phi^2}{1 + \phi^2} \tag{22c}$$

$$I_P^x = \sum_m \frac{[(J + 1)^2 - m^2][(J + 2)(J + 3) + m^2]}{2(2J + 1)^2(2J + 3)(2J + 5)} \frac{2 + \phi^2}{1 + \phi^2} \tag{22d}$$

where $\phi = \mu FM[(J + 1)(J + 2)]^2$. The summations extend from -J to +J, where J refers to the initial ground-state rotational level. Q- and P-branch intensity ratios for R(2), R(8), and R(14) excitation are plotted as a function of the reduced field, μF/q, in Fig. 18.

Several conclusions can be drawn: 1) Iq/Ip becomes field independent at larger fields for larger J since $\phi \sim J^{-4}$; 2) for unpolarized LIF, the limiting value of Iq/Ip is ∿ 2 because the Q-branch borrows from both R
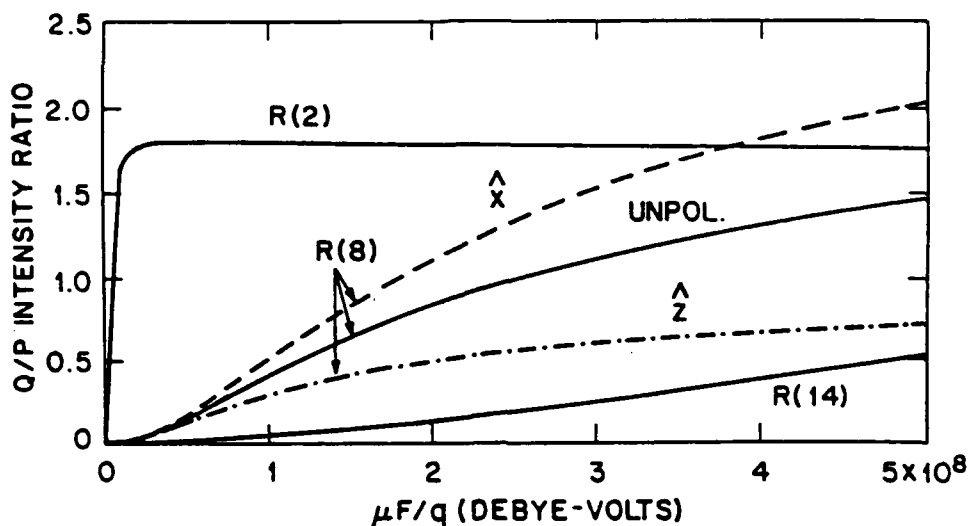
43

Figure 18. Calculated Q- to P-Branch Intensity Ratios
for R(2), R(8), and R(14) Pump Transitions
as Function of Reduced Electric-Field
Strength (from Ref. 6).

and P branches; 3) in the absence of collisions and hyperfine interac-
tions, the Q branch is polarized differently from P to R and, thus, e-f
mixing should be most prominent when x-polarized fluorescence is
detected; and 4) for a dipole moment of 1D and a Λ-doubling constant of
$2.5 \times 10^{-5}$ cm$^{-1}$, the minimum detectable field strength is ∿ 20 V/cm, if
it is assumed that a ratio of $Iq/Ip$ of 0.10 can be measured when R(2) is
excited.

The experimental arrangement for this study is shown in Fig. 19. The
output from a Lambda-Physik dye laser is frequency doubled and passed
through the discharge call. The LIF signal is collected at a right
angle to the dye-laser beam and directed to a J-Y 0.6-m monochromator
for filtering. The signal is detected by an S-20 photomultiplier and
fed into a PAR boxcar integrator. The boxcar signal is digitized and
stored on a PDP-11/23 micro-computer for analysis.

Initial experiments with this setup were unsuccessful. While the natu-
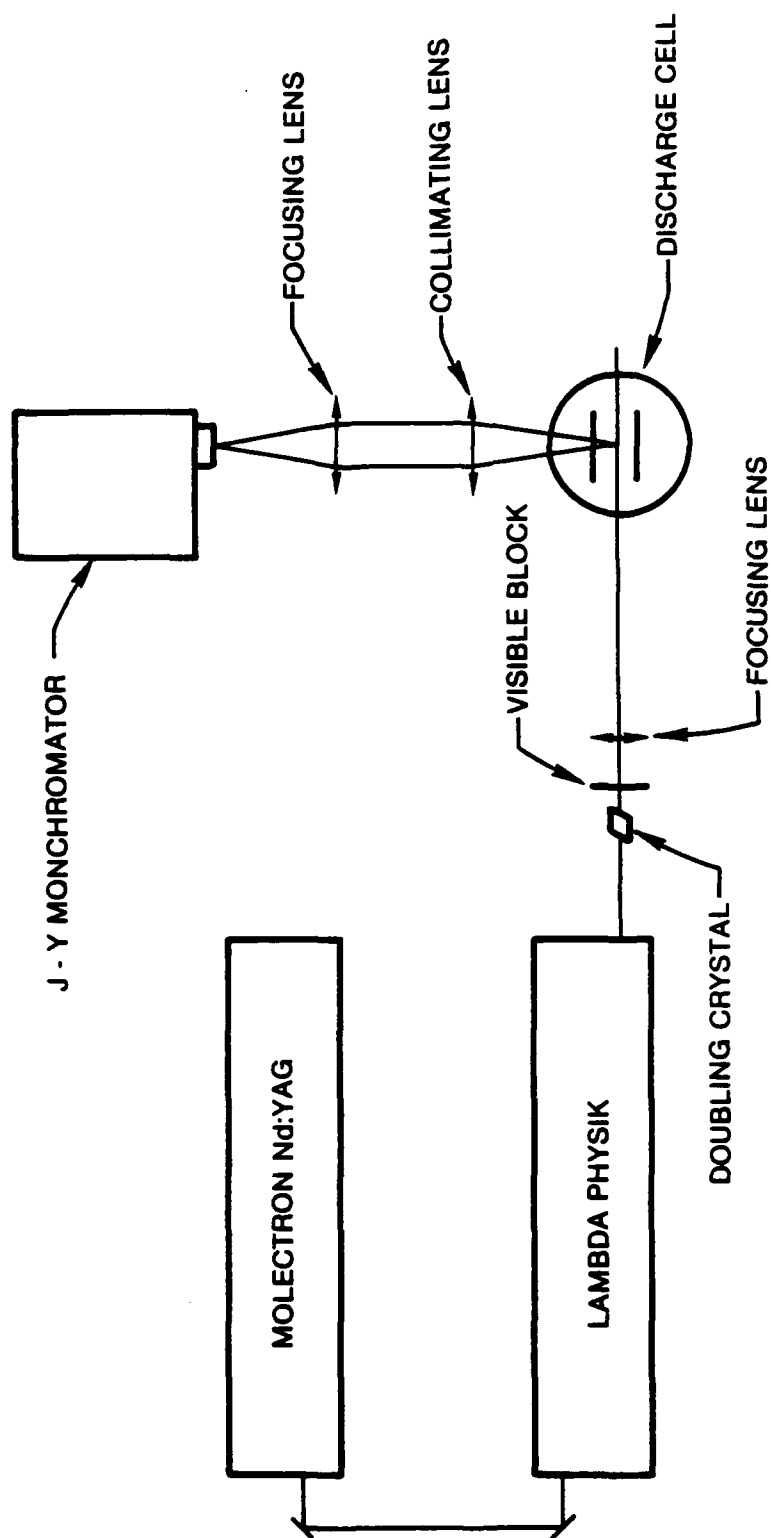ral emission of the BCl radical could be observed in the discharge glow,

Figure 19. Experimental Arrangement for BCl Fluorescence Study.

45

no LIF signal was observed. The discharge was operated at 10-Torr pressure during these experiments. The earlier work of Moore, et al.,[6] utilized an rf-pumped discharge at a pressure of < 1 Torr.

Quenching of the fluorescence appeared to be a severe problem in applying the technique to this discharge. A second serious problem was the strong contamination which occurred upon operating the discharge for long periods of time with the $BCl_3$ seeded gas. While this method apparently works well with rf low-pressure discharges, quenching and contamination limit its use in other discharge systems.

# REFERENCES

1. K. A. Safinya, J. F. Pelpech, and T. F. Gallagher, Phys. Rev. 22, 1062 (1980).

2. C. H. Townes and A. L. Schawlow, Microwave Spectroscopy (Dover Publications, New York, 1975).

3. H. A. Bethe and E. E. Salpeter, Quantum Mechanics of One and Two-Electron Atoms (Academic Press, Inc., New York, 1975).

4. G. Luders, Ann. Phys. 6, 308 (1951).

5. J. S. Foster, Proc. Roy. Soc. (London) 117, 137 (1938).

6. C. A. Moore, G. P. Davis, and R. A. Gottscho, Phys. Rev. Lett. 52, 538 (1984).

7. T. W. Hansch, M. H. Nayfeh, S. A. Lee, S. M. Curry, and I. S. Shahin, Phys. Rev. Lett 32, 1336 (1974).

8. M. S. Sorem and A. L. Schawlow, Opt. Comm. 5, 148 (1972).

9 R. R. Freeman, P. F. Liao, R. Panock, and L. M. Humphrey, Phys. Rev. A 22, 1510 (1980).

10. J. E. Lawler, A. I. Ferguson, J. E. M. Goldsmith, D. J. Jackson, and A. L. Schawlow, Phys. Rev. Lett 42, 1046 (1979).

11. D. K. Doughty and J. E. Lawler, Appl. Phys. Lett. 45, 611 (1984).

12. High Resolution Laser Spectroscopy (K. Shinoda, Ed.) (Springer-Verlag, Berlin, 1976).

13. K. C. Harvey, R. T. Hawkins, G. Meisel, and A. L. Schawlow, Phys. Rev. Lett. 34, 1073 (1975).

14. L. A. Bloomfield, H. Gerhardt, and T. W. Hansch, Phys. Rev. A 27, 850 (1983).

15. C. Weiman and T. W. Hansch, Phys. Rev. Lett 36, 1170 (1976).

16. W. Demtroder, Laser Spectroscopy Basic Concepts and Instrumentation (Springer-Verlag, Berlin, 1982).

17. R. Dailey (University of California, Berkeley, CA), Private Communication.

18. E. W. Weber, Phys. Rev. A 20, 2278 (1979).

19. J. E. Lawler, Phys. Rev. A 22, 1024 (1980).

20. W. K. Schuebel, IEEE J. Quantum Electron. QE-6, 574 (1970).

21. D. H. Katayama, J. M. Cook, V. E. Bundybey, and T. A. Miller, Chem. Phys. Lett. <u>62</u>, 542 (1979).

22. D. K. Doughty, S. Salih, and J. E. Lawler, Phys. Lett. A <u>103</u>, 41 (1984).

23. B. N. Ganguly and A. Garscadden, Appl. Phys. Lett. <u>46</u>, 540 (1985).

24. B. N. Ganguly, B. L. Preppernau, and A. Garscadden, AIAA Paper No. 85-1638.